MATEUS ALVES ARAÚJO CRUZ

MULTI-DISCIPLINARY DESIGN OPTIMIZATION FOR CONCEPTUAL DESIGN OF HYBRID-ELECTRIC AIRCRAFT

UNIVERSIDADE FEDERAL DE UBERLÂNDIA
FACULDADE DE ENGENHARIA MECÂNICA
2019

MATEUS ALVES ARAÚJO CRUZ

MULTI-DISCIPLINARY DESIGN OPTIMIZATION FOR CONCEPTUAL DESIGN OF HYBRID-ELECTRIC AIRCRAFT

Course Completion Project submitted to the Department of Mechanical Engineering – FEMEC-UFU, in partial fulfillment of the requirements for the bachelor degree in Aeronautical Engineering. *FINAL VERSION*

Advisor: Prof. Dr. Thiago Augusto Machado Guimarães

Co-advisor: Eng. Me. Higor Luis Silva

Uberlândia - MG

2019

MATEUS ALVES ARAÚJO CRUZ

OTIMIZADOR MULTIDISCIPLINAR PARA PROJETO CONCEITUAL DE AAERONAVES HÍBRIDAS-ELÉTRICAS

Projeto de Conclusão de Curso apresentado à Faculdade de Engenharia Mecânica – FEMEC-UFU, como parte dos requisitos para obtenção do título de Bacharel em Engenharia Aeronáutica. *VERSÃO REVISADA*

Orientador: Prof. Dr. Thiago Augusto Machado Guimarães

Coorientador: Eng. Me. Higor Luis Silva

Uberlândia - MG

2019

To my family.

ACKNOWLEDGEMENTS

.

Firstly, I would like to thank God for beeing with me on every step of the way. I am also grateful for my family, especially my parents Fábio Cruz and Silvia Cruz and my sister Rebecca Cruz, for their endless support during my journey and life.

I would also like to thank the guidance given by the Professor Dr. Thiago Guimarães in this work and research conducted over the last two years.

I would like to thank Higor Silva, for the years of partnership in LPAA and his advisoring on my works. Additionally, to my friends at UFU Racing Formula Team for all the knowledge transmitted that goes beyond the ones given in class. Certainly I will be a better engineer because of this. And to my friends Alessandra Lopes, Igor Sousa, Fabio Machado, Lucca Peres, Luis Felipe Oliveira and Lucas Parreira for all the moments we lived together along this way.

And finally, I would like to thank the Examining Committee for the time spent evaluating this work.

Mateus Cruz

“Imagination is more important than knowledge”
Albert Einstein

RESUMO

CRUZ, M. A. A. **Otimizador Multidisciplinar para Projeto Conceitual de Aaeronaves Híbridas-elétricas**. 2019. 85 p. Projeto de Conclusão de Curso (Graduação em Engenharia Aeronáutica) – Faculdade de Engenharia Mecânica, Universidade Federal de Uberlândia, Uberlândia – MG, 2019.

O presente trabalho apresenta uma otimização de projeto multidisciplinar (MDO) para aviação geral e design de aeronaves híbridas-elétricas, integrando ferramentas de aerodinâmica, estruturas, mecânica de vôo e desempenho. Trazendo, ainda, as diferentes arquiteturas de projeto híbrido-elétrico. As metodologias usadas em cada caixa são apresentadas e, de forma geral, todas as ferramentas foram elaboradas de forma a utilizar pouco ou nenhum dado histórico, favorecendo o design de novos conceitos. A aeronave projetada está no mercado de aviação geral e os requisitos são especificados de acordo com seus concorrentes, tomando crédito de um sistema de propulsão distribuída. Além disso, as funções objetivas do MDO são minimizar o consumo de combustível e o peso máximo da decolagem.

Os resultados, no que tange a geometria, parâmetros aerodinâmicos e de desempenho são comparados com os concorrentes para validação. Por fim, o MDO é utiizado para gerar um projeto final de forma a evidenciar as relações de compromisso de uma aeronave híbrida-elétrica para os atuais objetivos impostos.

Palavras-chave: Otimização de Projeto Multidisciplinar, Aviação Geral, Aeronaves Híbridas-Elétricas, Propulsão Distribuída.

ABSTRACT

CRUZ, M. A. A. **Multi-disciplinary Design Optimization for Conceptual Design of Hybrid-Electric Aircraft**. 2019. 85 p. Projeto de Conclusão de Curso (Graduação em Engenharia Aeronáutica) – Faculdade de Engenharia Mecânica, Universidade Federal de Uberlândia, Uberlândia – MG, 2019.

This work presents a multidisciplinary design optimization (MDO) for general aviation and hybrid-electric aircraft design integrating boxes of aerodynamics, structures, flight mechanics and performance. The methodologies used in each box are presented and, to increase the reliability on new designs, these tools were made to minimize or not use at all any historical data. The aircraft designed is present in the general aviation market and the requirements are specified according to its competitors, taking credit of a distributed propulsion system. Furthermore, the objective-functions are minimize fuel consumption and maximum takeoff weight.

The results in terms of geometry, aerodynamic parameters and performance were compared to the aircraft competitors to evaluate the accuracy of the MDO. At least, the MDO generated a final project in order to highlight the commitment relationships of a hybrid-electric aircraft in matters of the objectuve-functions definded to this project.

Keywords: Multidisciplinary Design Optimization, General Aviation, Hybrid-Electric Aircraft, Distributed Propulsion.

LIST OF FIGURES

LIST OF TABLES

LIST OF SYMBOLS

b — Wingspan

C_D — Drag coefficient

$C_{D,0}$ — Parasite drag coefficient

C_L — Lift coefficient

$C_{L_{\text{HT}}}$ — Horizontal tail lift coefficient

$C_{L_{\text{max}}}$ — Maximum lift coefficient

C_m — Moment coefficient

C_{n_i} — Induced yaw coefficient

D — Drag

D_0 — Parasite Drag

D_i — Induced Drag

D_p — Propulsor diameter

e_b — Specific energy of battery

e_f — Specific fuel energy

H_E — Degree of hybridization for energy

H_P — Degree of hybridization for power

I — Moment of Inertia

L — Lift

L_{airframe} — Lift due to airframe

M — Mach number

MS_{VM} — Margin of safety for Von Mises criterion

N — Number of propulsors

P — Power

P_{bat} — Battery power

P_f — Fuel power

P_{gt} — Gas turbine power

S — Wing area

S_e — Elevator area

S_{HT} — Horizontal tail area

S_{VT} — Vertical tail area

T — Total thrust

T_{dp} — Thrust due to installed distributed propulsion

V_{md} — Speed of minimum drag

V_{HT} — Horizontal tail volume ratio

V_{VT} — Vertical tail volume ratio

W_{bat} — Battery weight

W_{em} — Electric motor weight

W_{empty} — Empty weight

W_{fuel} — Fuel weight

W_{gt} — Gas turbine weight

W_{PL} — Payload weight

W_{PT} — Powertrain weight

W_{TO} — Takeoff weight

W/S — Wing Load

α — Angle of attack

α_{HT} — Horizontal tail angle of attack

ΔD_0 — Parasite Drag Addition

ΔD_i — Induced Drag

ΔL — Lift Addition

Δt — Time variation

$\Delta y/b$ — Wingspan occupied by the DP array

$\Delta\eta_{dp}$ — Increase in efficiency due to distributed propulsion

ε — downwash angle

η_{dp} — Distributed propulsion efficiency

η_{HT} — Ratio between wing and tail aerodynamic pressure

ρ — Air density

ρ_{SL} — Air density at sea-level

σ — Normal stress

σ — Normal stress on Von Mises criterion

φ — Shaft power ratio

Φ — Supplied power ratio

τ — Elevator effectiveness parameter

τ_{bi} — Shear flow

CONTENTS

CHAPTER

1

INTRODUCTION

Fossil fuel alternatives have been a demand in recent years in all branches of industry. The growing concern with the environment has been a factor in this search, due to the highly polluting nature of this type of fuel (ANDRES *et al.*, 2011). Also, the growing demand of energy, the uncertainties about oil availability worldwide, and the instabilities in the Middle East tend to contribute to the increase of this energy source price.

Against this need, the study and development of fully or partially electric aircraft has been one of the stakes of the aircraft industry and universities over the last few years (SILVA *et al.*, 2019). This proposal leads to researches of new technologies to enable the development of previously unfeasible concepts.

In order to make this new concepts more viable, by reducing research and implementation costs, a multidisciplinary approach is proposed.

Multi-disciplinary design optimization (MDO) allows the incorporation of all relevant disciplines simultaneously using optimization methods to solve design problems, increasing the efficiency of designs to be optimized, resulting in a reduction of time cycles and costs of the project (SOBIESZCZANSKI-SOBIESKI; HAFTKA, 1997).

The use of multiple simulations is a key concept of MDO. This involves several tools, such as fluid flow solvers, structural analysis, cost modelling and tools for design and reliability. Although there are tools and softwares that are highly effective individually, the challenge now is to provide the right tools to support this integrated approach.

At a general level, when considering the overall mission performance of an aircraft, the tool is used during the early stages of the project (KROO *et al.*, 1994). However, currently most MDO applications are based on major simplifications in mathematical modelling, such as beam structural models or panel methods for aerodynamics.

Along those lines, this work presents a MDO method for conceptual design of general

aviation and hybrid-electric aircraft. The MDO comprises boxes of engineering that includes aerodynamics, flight mechanics, structures, and performance, integrating all of them. After validating the accuracy of the aerodynamic and flight mechanics solvers, a case study is presented.

1.1 Document Structure

This document is structured, as follows:

- Chapter 2 presents the main concepts around multidisciplinary optimization methods, general aviation, hybrid-electric aircraft and distributed propulsion systems;
- Chapter 3 describes the MDO premises, operations and its components. Moreover, it presents the approaches of each component, such as structural and aerodynamics analysis, flight mechanics and the aircraft mission;
- Chapter 4 brings the confrontation between the MDO's results and others licensed softwares in order to validate and test the accuracy of the developed MDO;
- Chapter 5 summarizes a case study to demonstrate the operation and results of the method;
- Chapter 6 presents the main conclusions of the method, approaches and propositions in this work, and proposals for future work.

CHAPTER

2

LITERATURE SURVEY AND THEORY

2.1 Multidisciplinary Design Optimization

Multidisciplinary design optimization (MDO) is a field of engineering that uses optimization methods to solve design problems incorporating multiple disciplines or subsystems. The main advantage of this method is that the optimal design of a multidisciplinary system can only be found when the interactions between the disciplines are fully considered. Even that bringing all these disciplines together increases the complexity of the problem, the optimum solution is way superior than the one found by optimizing each discipline sequentially (KROO *et al.*, 1994).

One of the first applications of an MDO was an aircraft wing design considering three strongly coupled fields: aerodynamics, structures and controls. Since then, MDO approaches kept evolving until it was used to solve more challenging problems such as an entire aircraft (SOBIESZCZANSKI-SOBIESKI; HAFTKA, 1997). Also, this method have invaded the others fields of engineering, such as automobile design, naval architecture, and electronics, and started being used in a greater scale.

The main concerns around the implementation of an MDO are how to organize the disciplinary analysis models, the optimization software in according with the problem formulation so that the optimal design is achieved and the approximations models. Such strategy in combination with the problem formulation defines the MDO architecture, defining how the different models are going to interact and how the overall optimization problem is solved.

There are many different architectures that can be used to solve a given optimal design problem, and choosing the most appropriate architecture for the problem can reduce significantly the time solution. The selected methods for solving each discipline and the coupling scheme used in the architecture are definitive to save time in each iteration. These considerations become more important as the design becomes more complex, detailed and the number of variables and constraints increases.

2.1.1 Variables and Constraints

A design variable is a specification that is controllable from the point of view of the designer and it is always under the explicit control of an optimizer. These variables can be continuous, discrete or boolean. They also may pertain only to a single discipline or may be shared by multiple disciplines.

Constraints, just like the design variables, are defined by the design team and they are a condition that must be satisfied to make the design feasible. These constraints can reflect a physical law, bounds or just user requirements. Constraints can be used explicitly by the solution algorithm or can be incorporated into the objective.

Design problems with continuous variables are normally solved more easily; however, with an elevated number of design variables and constraints, the problem becomes more complex and, therefore, demands more processing power and time to be solved. Also, the design variables are often coupled; in other words, the value assumed by one variable will affect another variable creating the necessity of more cycles to find the optimal outcome.

2.1.2 Objectives

An objective is a numerical value to be maximized or minimized according to the will of the design team or final objective of the project.

Multiple objectives can be defined, however, more objectives requires more computational capability and time. Also, many solution methods works only with single objectives. So, when using these methods or looking for minimize the elapsed time, the design team needs to weight the various objectives and sum them to form a single objective often by sacrificing the possibility to find a more optimal design result.

2.1.3 MDO Methods

Numerical optimization reached prominence in the digital age, although Isaac Newton, Leonhard Euler, Daniel Bernoulli and Joseph Lagrange already had used them to solve problems. Its systematic application to structural design dates to the 60s when used by Schmit and Haftka. The success of structural optimization on the next years motivated the emergence of multidisciplinary design optimization in the 1980s. First, the popular gradient-based methods used by the early structural optimization and then MDO practitioners have investigated optimization methods in several broad areas. These include decomposition methods, approximation methods, evolutionary algorithms, memetic algorithms, response surface methodology, reliability-based optimization, and multi-objective optimization approaches.

2.1.3.1 Genetic Algorithm

In a Genetic Algorithm (GA), a population of candidate solutions to an optimization problem evolves toward better solutions (DATTA, 2012). The evolution usually starts from a population of randomly generated individuals, and it is an iterative process, with the population in each iteration being called a generation. In each generation, the fitness of every individual in the population is evaluated; the fitness is usually the value of the objective function in the optimization problem being solved. The more fit individuals are statistically selected from the current population, and each individual's genome is modified (recombined and possibly randomly mutated) to form a new generation. The new generation of candidate solutions is then used in the next iteration of the algorithm. Commonly, the algorithm terminates when either a maximum number of generations has been produced, or a satisfactory fitness level has been reached for the population. The Figure 1 represents a common flow for this type of algorithm.

Figure 1 – Flowchart of Genetic Algorithm.

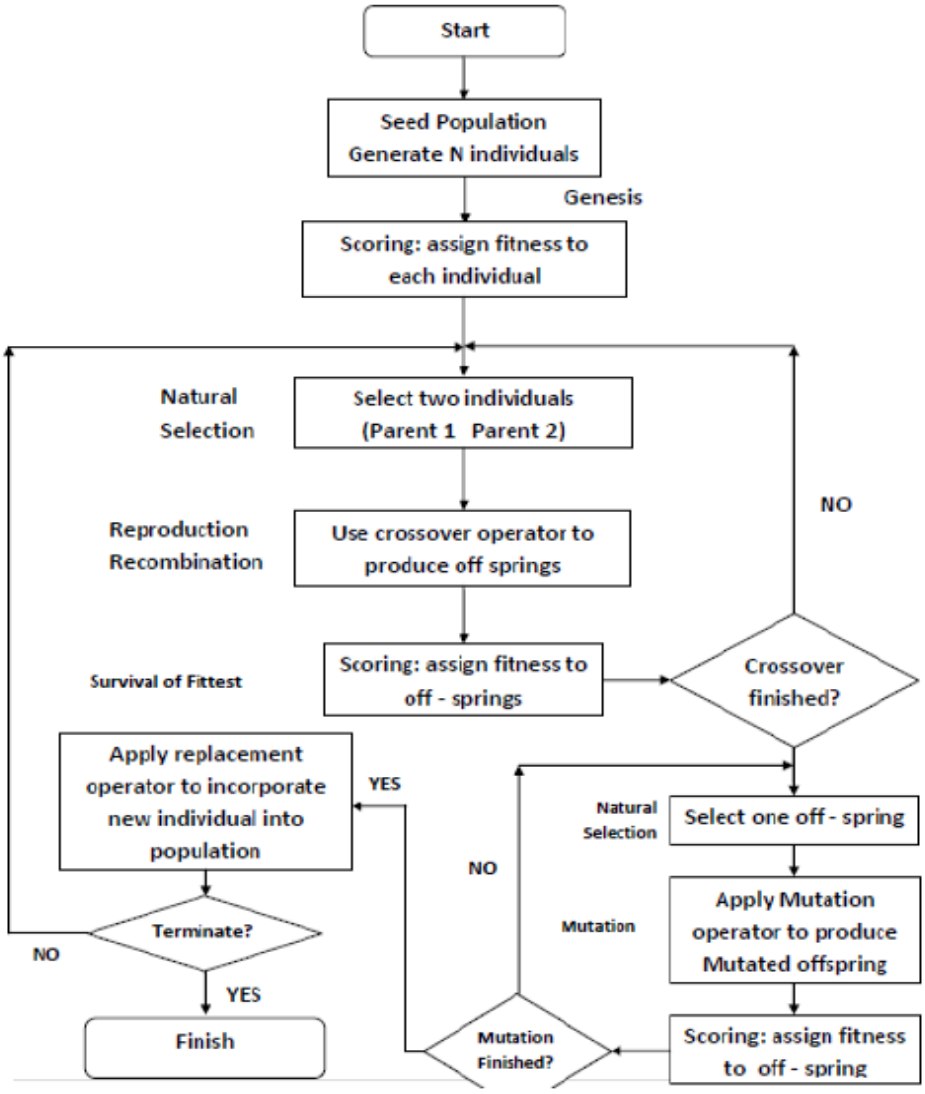

Source: Datta (2012).

A typical genetic algorithm requires a genetic representation of the solution domain and a fitness function to evaluate the solution domain.

The population size depends on the nature of the problem, but typically contains several hundreds or thousands of possible solutions. Often, the initial population is generated randomly, allowing the entire range of possible solutions (the search space). Occasionally, the solutions may be "seeded" in areas where optimal solutions are likely to be found.

During each successive generation, a portion of the existing population is selected to breed a new generation. Individual solutions are selected through a fitness-based process, where fitter solutions (as measured by a fitness function) are typically more likely to be selected. Certain selection methods rate the fitness of each solution and preferentially select the best solutions. Other methods rate only a random sample of the population, as the former process may be very time-consuming.

The fitness function is defined over the genetic representation and measures the quality of the represented solution. In some problems, it is hard or even impossible to define the fitness expression; in these cases, a simulation may be used to determine the fitness function value of a phenotype (e.g., computational fluid dynamics is used to determine the air resistance of a vehicle whose shape is encoded as the phenotype), or even interactive genetic algorithms are used.

The next step is to generate a second generation population of solutions from those selected through a combination of genetic operators: recombination and mutation. For each new solution to be produced, a pair of "parent" solutions is selected to produce a "child" solution using the recombination and mutation methods, a new solution is created which typically shares many of the characteristics of its "parents". New parents are selected for each new child, and the process continues until a new population of solutions of appropriate size is generated.

This generational process is repeated until a termination condition has been reached like when a solution is found that satisfies minimum criteria or the fixed number of generations is reached.

2.1.3.2 Differential Evolution

First proposed in 1997 by Storn and Price, Differential Evolution (DE) is a simple yet effective algorithm for global (multimodal) optimization. Although primarily designed for optimizing functions of continuous and discrete numerical variables, DE has also been applied with some success to combinatorial problems.

DE belongs to the class of Evolutionary Algorithms (EAs), so-called because they are population-based methods that rely on mutation, recombination and selection to evolve a collection of candidate solutions toward an optimal state (PRICE, 2013). Like most EAs, DE exploits the population via recombination. DE does not, however, attempt to mimic natural searches, like those of ants, bees, the immune system, or those arising from social interaction.

Furthermore, only DE directly samples the population to drive mutation – a strategy that has many benefits.

2.2 Hybrid-Electric Aircraft

Looking forward to create greener technologies, engineers and researches have spent time developing new designs concept in aviation. One of this new technologies are the fully or partially electric aircraft that will reduce the use, or not use at all, fossil fuels as energy source. Reducing the use of this type of energy source has more advantage than only reduce the carbon dioxide (CO_2) emissions, but also brings reductions in the operational costs of the aircraft and maintenance costs are reduced as well.

Such an effort, to develop greener technologies, comes with the increasing environmental concern around the world and the pressure applied by institutions to push the industries forward into this greener future. One of this institutions is the National Aeronautics and Space Administration - NASA that launched a series of targets, represented in Figure 2 to be accomplished by the aerospace industry.

Figure 2 – Targets recommended by NASA

Table 1. NASA subsonic transport system level metrics.

CORNERS OF THE TRADE SPACE	N+1 (2015)*** Technology Benefits Relative to a Single Aisle Reference Configuration	N+2 (2020)*** Technology Benefits Relative to a Large Twin Aisle Reference Configuration	N+3 (2025)*** Technology Benefits
Noise (cum below Stage 4)	- 32 dB	- 42 dB	- 71 dB
LTO NOx Emissions (below CAEP 6)	-60%	-75%	better than -75%
Performance: Aircraft Fuel Burn	-33%**	-50%**	better than -70%
Performance: Field Length	-33%	-50%	exploit metroplex* concepts

*** Technology Readiness Level for key technologies = 4-6
** Additional gains may be possible through operational improvements
* Concepts that enable optimal use of runways at multiple airports within the metropolitan areas

Source: Kim (2010).

Therefore, it is of great interest that electric flights becomes real, but this type of fight is highly dependent and related to the energy storage technology available (SILVA *et al.*, 2019). Also, due to its purpose of being used in the aerospace industry, this storage technology needs to be light, compact, safe and reliable. Within this design philosophy, the most feasible technology is the battery. However, batteries must be able to meet both power density and energy density requirements, as well as they must be able to show high convenience from an economical and ecological point of view (KUHN; SIZMANN, 2012).

2.2.1 Batteries

Some concepts and terminologies regarding batteries are important to come up with, as follows:

- Specific Energy [Wh/kg]: it is also known as gravimetric energy density, and it is defined as the amount of electrical energy stored for unit battery mass. Thus, it is dependent on battery chemistry and packaging;

- Specific Capacity [Ah/kg]: it represents the Amp-hours available when the battery discharges at a certain current, per unit of mass. Similar to the specific energy, limits to the discharge current are given by the cell chemistry and its weight is influenced both by the materials necessary in the electrochemical process as well as the packaging of the cells;

- Specific Power [W/kg]: dependant on chemistry and packaging, it determines the weight required to reach a given performance. There is a strong trade-off between specific energy and specific power for high discharge rates during high power demands, in which the battery capacity drops very fast, significantly reducing the specific energy;

- Energy Density [Wh/m^3] or [Wh/l]: along with the energy consumption of the vehicle, it determines the volume occupied by the battery, being a function of packaging and chemistry;

- Stored Energy [Wh] or [J]: the energy stored is equal to the product of the battery voltage V and the capacity Q [Ah]. The stored energy is a function of how quickly a battery is charged or discharged as with increasing currents the internal losses grow;

- State of Charge (SOC) [%]: it is defined as the ratio between the remaining capacity and the nominal capacity. It goes from 100% (fully charged) to 0% (fully discharged), but batteries usually have a practical lower SOC limit under which the cells are permanently damaged. This limit is usually around SOC = 20-30% for modern Li-Ion batteries;

- Depth of Discharge (DoD) [%]: it is the rate of discharged capacity over the nominal capacity. It is also defined as DoD = 1-SOC.

- Cost [$/Wh]: depending on the cost of raw materials and industrial processes required to manufacture the battery.

CINAR *et al.* states that studies performed by Safran company show that for commuter applications the battery-level specific energy should be, at least, 500 Wh/kg, while studies on larger aircraft conducted by Boeing show the need of at least 600-750 Wh/kg.

2.2.1.1 Battery types

Lithium-ion and Lithium-polymer batteries are the most common batteries due to very high performance compared to other technologies available on the market. Its specific energy is around 150 Wh/kg while the energy density can be as high as 650 Wh/l. However, when it comes to safety, these batteries can be dangerous due to chances of explosion.

The Li-air (or Li-O_2) batteries are quite promising, possibly having specific energy values around 11500 Wh/kg, which is very close to the aviation fuel specific energy of 11900 Wh/kg. However, this kind of battery has some safety issues, has limited life cycles and its charged and discharged rates are not very competitive with the other types of battery.

The Lithium-Sulfur batteries are already available with specific energies around 250 Wh/kg; however, there is a prototype with a specific energy of 600 Wh/kg and a power density of 150 Wh/l already being tested in laboratory. On the other hand, they have low life-cycle and low efficiency that does not permit the full extraction of the chemical energy.

Regarding the future of these technologies, GERSSEN-GONDELACH; FAAIJ gathered the predictions and expectations for the characteristics and performances of the batteries for the year 2025, being updated to 2035 by (ZAMBONI *et al.*, 2019), which are available in Table 1.

Table 1 – Numeric values for aerodynamic solver validation.

	Li-ion	Li-S	Li-air
Specific Energy [Wh/kg]	250-350	600-700	800-1500
Specific Power [W/kg]	500-600	350-500	300-400
Energy Density [Wh/l]	600-800	300-350	1000-1700
Charge/Discharge efficiency [%]	90-95	70-90	60-85
Cycle life [# cycles]	1000-3000	1000-2500	500-1000
Degree of Discharge [%]	70-90	90-100	70-90
Lifetime [years]	7-15	7-14	5-10
Cost [$2010]	250-350	250-500	400-800
Uncertainty	low	medium	high

Source: Silva *et al.* (2019).

Li-S and Li-air batteries should probably be the best options for future projects, since they can achieve high specific energy levels. However, there are still major challenges to board these batteries on a plane, such as project maturity, redundancy in operational safety, flammability testing, i.e., all that is necessary to ensure safety and reliability requirements.

2.2.2 Fundamentals and Architectures

The supplied power ratio (Φ) , which is defined as the total electric motor power over the entire mission in relation to the total shaft power over the entire mission as show in Equation 2.1,

is the best parameter to measure the hybridization level of the design. Also, two other parameters that shows the degree of hybridization is the ones that relate energy (H_E) and power (H_P)

$$\Phi = \frac{P_{em_{total}}}{P_{shaft_{total}}} \tag{2.1}$$

$$H_E = \frac{E_{electric}}{E_{total}} \tag{2.2}$$

$$H_P = \frac{P_{electric}}{P_{total}} \tag{2.3}$$

The value of $\Phi = 0$ represents a conventional aircraft while the value of $\Phi = 1$ represents a fully electric aircraft.

Figure 3 displays an example functional correlation between installed H_P and H_E for a dual-energy storage-propulsion-power system (DESPPS) based upon kerosene and batteries as energy carriers targeting YEIS 2035 and were derived from assumed step values of Φ. Some cases of architectures are classified in Table 2 and represented in Fig. 4.

Figure 3 – Example of a Degree-of-Hybridization trade-study conducted for a hypothetical Dual-Energy Storage-Propulsion-Power System (YEIS 2035).

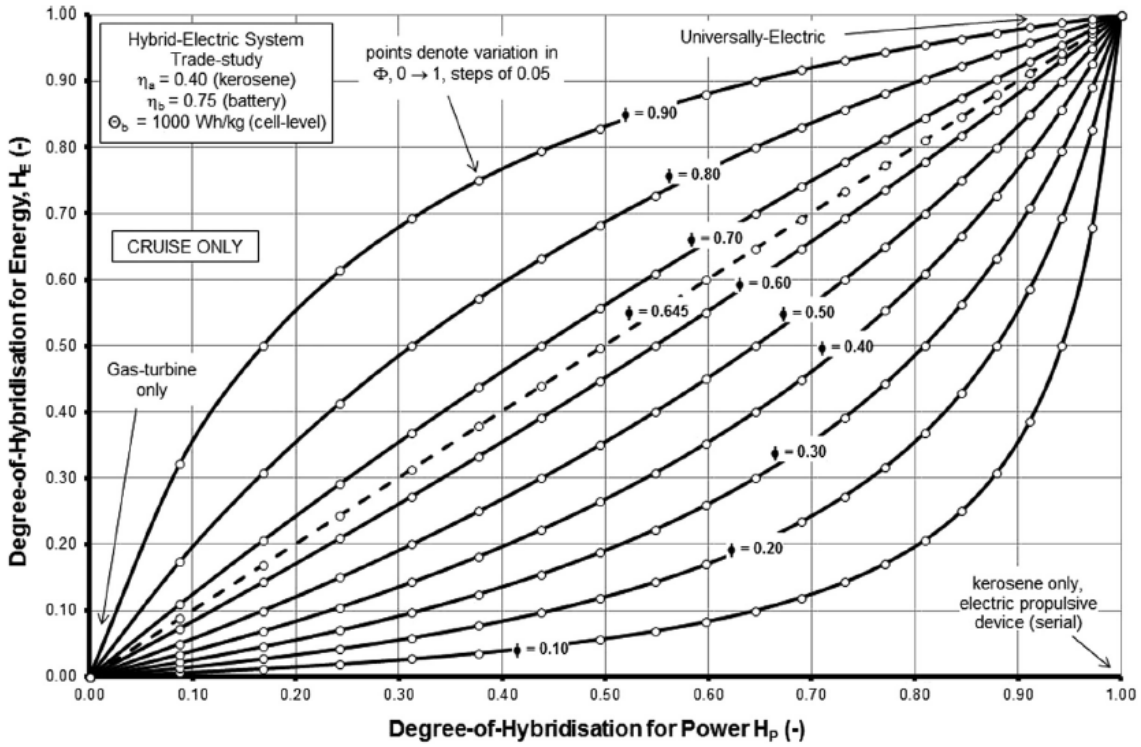

Source: Singh *et al.* (2014).

The all-electric aircraft have all the subsystems and the propulsion exclusively electric, i.e., powered by electric motors. Electricity may be supplied by a variety of methods including

Figure 4 – Simplified models of the different architectures considered.

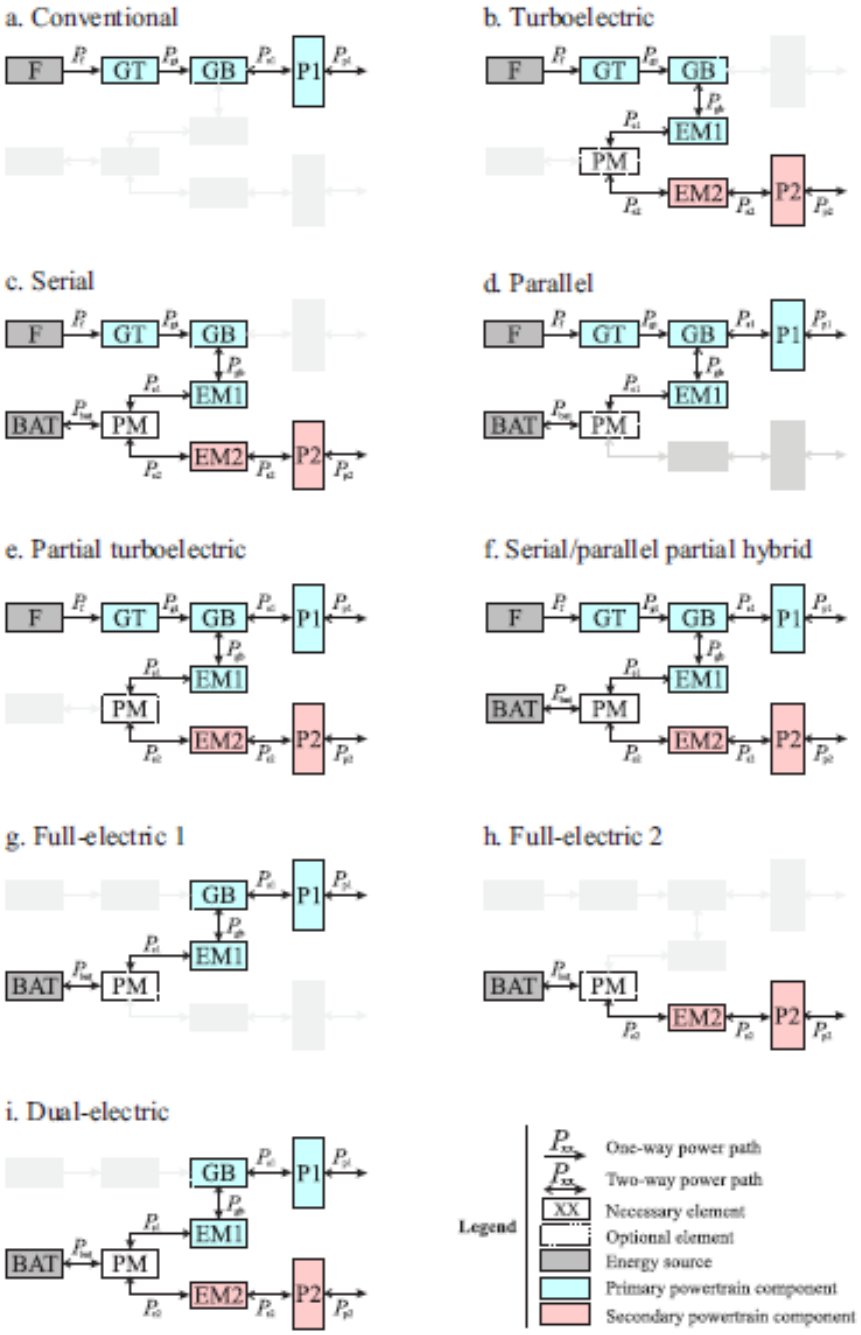

Source: Felder (2015).

batteries, ground power cables, solar cells, ultracapacitors, fuel cells, and power beaming.

In the series configurations, all the propulsive power is produced by electric motors. Depending on the degree-of-hybridization in terms of energy (HE), there is a difference between the pure serial (turboelectric) and the series hybrid. The turboelectric architecture (or pure series) is different when compared to other configurations because it does not depend on energy storage systems, such as batteries.

Parallel architectures has its engine and motor connected by a mechanical coupler. In this

configuration, different control strategies can be used. If the power required by the transmission is higher than the output power of the engine, the electric motor is turned on so that both engines can supply power to the transmission. If the power required by the transmission is less than the output power of the engine, the remaining power is used to charge the battery pack.

The series-parallel architecture is a combination of the advantages of the series and parallel configurations. However, there's a weight gain due to the increase of components required for this configuration.

The partial turboelectric architecture is very similar to the parallel-series architecture, differentiating by not including batteries in its layout.

Table 2 – Architectures characteristics.

Architectures	H_P	H_E
Conventional	0	0
All-Electric	1	1
Turboelectric	> 0	0
Series Hybrid	1	< 1
Parallel Hybrid	< 1	< 1

2.3 Distributed Propulsion

Just like the hybrid-electric aircraft motivation, engineers and researchers are also looking for new propulsive configurations in an attempt to extract more benefits than just the ones from the propulsive system itself.

The Distributed Propulsion System (DPS) consists in the distribution of the propulsive elements (propellers, fans and jets) along most part of the wing as show in the NASA Prototype presented in Figure 5, is one of this possible configurations and its benefits, stated by KIM, can be many as follows:

- Reduction in fuel consumption by ingesting the thick boundary layer flow and filling in the wake generated by the airframe with the distributed engine thrust stream
- Spanwise high lift via high-aspect-ratio trailing-edge nozzles for vectored thrust providing powered lift, boundary layer control, and/or supercirculation around the wing, all of which enable short take-off capability.
- Better integration of the propulsion system with the airframe for reduction in noise to the surrounding community through airframe shielding.

- Reduction in aircraft propulsion installation weight through inlet/nozzle/wing structure integration.
- Elimination of aircraft control surfaces through differential and vectoring thrust for pitch, roll, and yaw moments.
- High production rates and easy replacement of engines or propulsors that are small and light.
- For the multi-fan/single engine core concept, the propulsion configuration provides a very high bypass ratio enabling low fuel burn, emissions, and noise to surrounding communities.

Figure 5 – NASA's prototype X-57 Maxwell.

Also, the combined effects of an hybrid-electric configuration and the distributed propulsion system presents more benefits when compared to a conventional propulsion system.

2.3.1 Sizing

Due to the system's influence in the aerodynamics of the aircraft, its contribution to lift and drag needs to be taken in account. So, the aircraft's total lift and drag are given by the Equations 2.4 and 2.5, respectively.

$$L = L_{airframe} + \Delta L(T_{dp}, L_{airframe}, S, ...) \tag{2.4}$$

$$D = D_0 + \Delta D_0(T_{dp}, S, ...) + D_i(L_{airframe}) + \Delta D_i(T_{dp}, L_{airframe}, S, ...) \tag{2.5}$$

where T_{dp} is the thrust generated by the new architecture, ΔL and ΔD_0 is the lift and drag addition provided by the DPS, respectively. Also, ΔD_i is the induced drag addition that is provided by

the installed system. Furthermore, the motor's position and the size of the propellers are also required. Using the method presented by VRIES; BROWN; VOS and it is represented in Figure 6.

Figure 6 – Propeller's sizing simplified model.

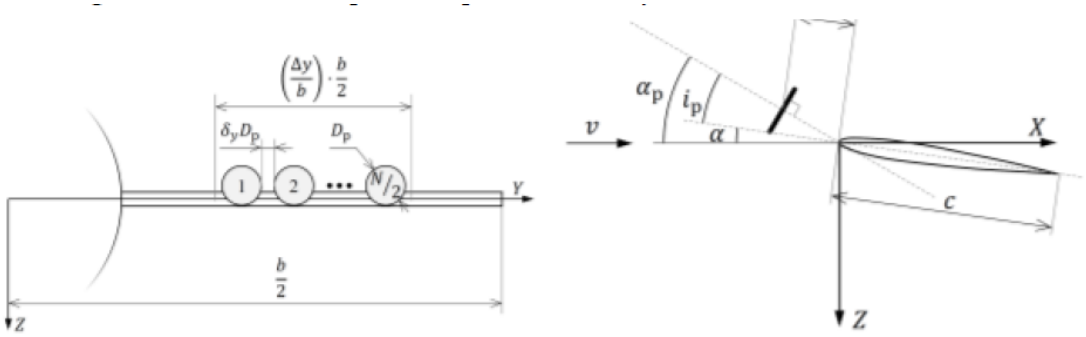

(a) Front view. (b) Sectional view.

Source: Vries, Brown and Vos (2018).

In this model, a simplified rectangular wing is taken into account with wingspan b and chord c. Half of the propellers are going to be placed in each semi wing ($\frac{N}{2}$). The propeller size (D_p) is determined by the Equation 2.6 and the space between two propellers is given by $\delta_y D_p$. No propellers is going to be placed in the wingtip or root and this distance is given by $\frac{\delta_y}{2}$. The designer defines N and $\delta_y D_p$.

$$D_p = \frac{b(\frac{\Delta_y}{b})}{N(1+\delta_y)} \tag{2.6}$$

CHAPTER

3

MULTIDISCIPLINARY OPTIMIZATION

The MDO proposed integrates the boxes of performance, aerodynamics, flight mechanics, and structures. Having the market and operational requirements, the MDO uses a genetic algorithm technique to optimize the aircraft in order to find it's best configuration that fits the constraints and the objective function.

For each aircraft under analysis, Fig. 7 presents the convergence process of an iteration. With the definition of requirements and design variables, the analysis begins with the constraint diagram. The determination of the wing loading (W/S) allows the calculation of the wing geometries. Then, the aerodynamic coefficients are evaluated through the aerodynamic solver.

Figure 7 – Illustration of the integration of the MDO boxes.

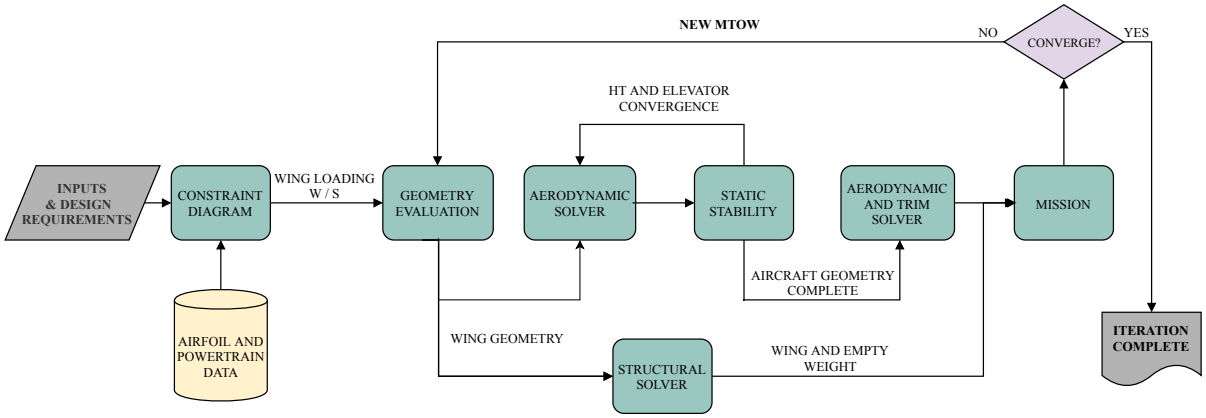

Source: SILVA *et al.* (2019).

The static stability box takes care of the sizing of the horizontal tail, vertical tail, and elevator using an iterative method integrated with the aerodynamic solver. Then, wing and empty weights are obtained through the structural box. Next, having the complete geometry defined, the aircraft's drag polar is computed, considering a trim condition, in order to feed the mission

module. The propulsive system is determined based on the power required and energy spent in each flight phase. Finally, the value of the maximum takeoff weight (MTOW) is updated, including all the weight breakdown (payload, powertrain, wing, battery, fuel, and airframe), and it goes back to the system so that a new wing geometry is defined.

At each iteration, this procedure repeats until there is a convergence in the MTOW value, aircraft geometry and configurations. The methodology applied in each box is presented in the following sections.

3.1 Constraint Diagram

The constraint diagram box evaluates the different performance constraints of the aircraft and generates a resulting feasible design space in terms of wing loading and thrust-to-weight ratio (or power loading). Then, from this feasible design space, it is possible to define the wing area and the installed power, which are, initially, the main step when designing an aircraft.

For this MDO, the mission requirements define the actual constraints. In addition, it is taken into account a distributed propulsive system, which comprises a set of electric propulsors usually installed along the wing, generating air-propulsive interactions that result in gains in propulsion and total-lift of the aircraft. Thus, after considering the "Deltas" of C_L and C_D, the optimum design point is chosen to generate the smallest wing; in other words, it means the point that delivers the highest wing loading (W/S). Finally, for a specific aircraft weight, this value of W/S feeds the geometry evaluation, which calculates the rest of the geometric parameters of the aircraft and so on.

3.1.1 Requirement and Constraints

In order to start the design, it is necessary to define its objective and requirements to define a design's baseline to evaluate key characteristics of the aircraft like its weight and size. The following is a typical set of requirements and technical objectives for jet transports:

- Payload: It is the requirement that drives the size of the aircraft, defining how much weight (or the number of passengers) the aircraft will carry. On personal and small general aviation aircraft, the pilot is considered as payload, unlike in business and commercial aircraft that the crew is part of the operative weight.

- Range: It is the maximum distance over which the payload can be transported without refueling and defines the required amount of energy to propel the aircraft over its mission profile.

- Cruise Speed/Altitude Capability: With these requirements is necessary to analyse, also, the ambient conditions to define then. However, the aircraft's speed drives the wing configuration and propulsion system choice.
- Takeoff Distance: It is the length of a runway needed to accelerate, lift off and climb to a prescribed obstacle height, like the 35 ft for commercial aircraft, imposed by the FAR Part 25.
- Climb Requirements: The Climb Rate is the vertical component of the airspeed of the aircraft during climbing. The Climb Gradient that is the ratio between the vertical and the horizontal traveled distances during the climb.
- Airport compatibility : It comprises the airfield classification, defining limitations to wing span and length, landing gear track and runway pavement loading.
- Environmental issues: It includes the maximum noise emission levels defined relative to certification requirements by, for example, FAR and ICAO.
- Reliability and Durability: Intense airliner utilization emphasizes the need to achieve a specified lifetime in terms of a number of flight hours and/or flight cycles.

For each mission, it is necessary to define the aircraft's best configuration, that includes wing position, tail configuration and engine location.

3.2 Aerodynamics

The aerodynamic package will be composed by potential flow-based solvers, such as Lifting Line Theory (LLT), Vortex Lattice Method (VLM) and Non-Linear Vortex Lattice Method (NL-VLM). These solvers are integrated with object-oriented variables in order to share its results - aerodynamic loads, coefficients, and derivatives - with the remaining areas of project in a standard way.

The potential-flow methods are based on the solution of Laplace's equation through the distribution of vortex singularities in a simplified version of the geometry and the imposition of boundary conditions. This methodology can only be applied for non rotational inviscid flows, though it is possible to approximate viscosity effects through the NL-VLM. Despite these restrictions, it presents low computational costs and enough accuracy to be used in optimization routines and preliminary projects.

The Non-Linear Vortex Lattice Method, firstly implemented by CARVALHO *et al.*, is capable of simulating generic sets of lifting surfaces over subsonic symmetrical or asymmetrical flow and maneuver speeds, considering interference between surfaces. This strategy is based on the correction of the inviscid three-dimensional solution by means of previously known bi-dimensional viscous section data, such as numeric simulation or experimental results.

3.2.1 Potential Flow

The simplified solution of flows around surfaces consists in the Prandtl's Boundary Layer Theory, that suggests a flow solution in two parts: the viscous region and the potential region. The viscous region is the one next to the body, where the viscous forces are predominant ($\mu \neq 0$), while in the potential region, located far from the body, the predominant ones are the inertial forces ($\mu \approx 0$). According to Prandtl, the Euler Equation defines the potential region and is know as:

$$\frac{\partial u_i}{\partial t} + \frac{\partial (u_i u_j)}{\partial x_j} = -\frac{1}{\rho}\frac{\partial p}{\partial x_i}. \tag{3.1}$$

However, a more convenient way to define the incompressible and inviscid region is by using the potential speed. In this regime, the flow does not suffer volume variation, so the divergent component is null:

$$\frac{\partial u_i}{\partial x_i} = 0. \tag{3.2}$$

Furthermore, if the flow is irrotational, the flow speed can still be expressed as a scalar function gradient, known as potential speed (ϕ):

$$\vec{V} = \nabla \phi \tag{3.3}$$

From the equation 3.2 and 3.3 the Laplace equation is obtained:

$$\nabla^2 \phi = 0 \tag{3.4}$$

Knowing that the equation 3.4 is linear, then it is possible to insert particular solutions to it and obtain new solutions.

3.2.2 Singularities Method

This method consists in the addition of a set of particular solutions into the equation 3.4 to obtain a new solution that is capable of representing the flow. Doing so, a discreet domain isn't necessary anymore resulting in a significant computational cost saving. Although this major simplification makes impossible to use this method in more complex geometries, it is still possible to use it for lifting surfaces in a initial phase project with satisfactory results.

For this work, there are two singularities of greater interest, the vortex and the uniform flow. A uniform flow with velocity V_∞ and moving in $\vec{x}$ direction can be represented by the

equation:

$$\phi = V_\infty \vec{x}. \tag{3.5}$$

A bi-dimensional vortex is a flow where all flow lines are concentric circles and the velocity at a point P is proportional to the distance to the center. The Laplace solution for this kind of flow is given by the equation 3.6 where Γ is the vortex intensity and θ is the point position as show in Figure 8.

$$\phi = -\frac{\Gamma}{2\pi}\theta. \tag{3.6}$$

Figure 8 – Vortex singularity representation.

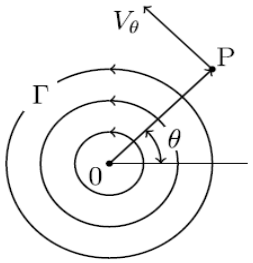

Source: Carvalho *et al.* (2018).

The vortex concept can be extend to tridimensional problems. In this cases, the vortex center would assume a filament geometry as Figure 9. Also, the filament induces a velocity field in the space around itself and the intensity is defined as Γ. The Biot-Savart law, expressed in Equation 3.7 can determine the induced velocity $\vec{dV}$ in a generic point P in the space, $\vec{dl}$ is filament's tangent vector and $\vec{r}$ is the distance between the point and the filament.

Figure 9 – Vortex Filament with intensity Γ.

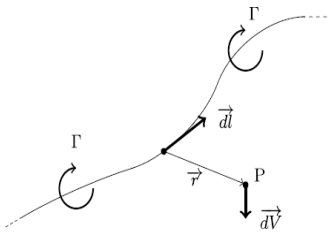

Source: Carvalho *et al.* (2018).

$$\vec{dV} = \frac{\Gamma}{4\pi}\frac{\vec{dl}x\vec{r}}{||\vec{r}||^3} \tag{3.7}$$

The Helmholtz Theorem brings two concepts about vortex:

- The intensity along the filament of the vortex needs to be constant;
- The vortex filament can not end inside it's own domain. It needs to extends itself until the borders ($\pm\infty$) or form a closed path commonly know as vortex ring.

As follows, a common type of vortex filament is the Horseshoe Vortex, represented in the Figure 10, it's composed by three vortex segments, one fixed and other two that are free and extends to the infinite.

Figure 10 – Horseshoe Vortex Representation.

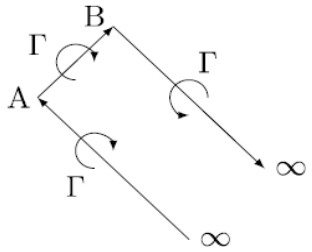

Source: Carvalho *et al.* (2018).

3.2.3 Vortex Lattice Method

Both Panel Method (HESS; SMITH, 1966) and Vortex-Lattice Method (MIRANDA; ELLIOTT, 1977) uses Laplace's Equation to solve the potential flow and distributing singularities throughout the body that meet the requirements of impermeability (the flow can't cross a solid surface) and the Kutta Condition.

The difference between both, however relay on the type of the used singularity.

They are fast and robust methods due to it's characteristics of solving the flow field over the surface of the body only. Allows multiples surfaces and calculating the interference that they provoke in each other. Also allowing complex geometries, angular velocity and sideslip angle. The formulation also permits to be added complementary models allowing boundary layer calculations and compressible flow corrections. Therefore, these definitive characteristics makes these methods to be the most used ones in computational aerodynamic tools.

For this solver, the wing is only discretized along the wingspan as the chords contributions are going to be added posteriorly. In this way, the chord will only have one horseshoe vortex along it. The fixed part of the vortex is at 1/4 of the chord and the control point (P) is at 3/4 of the chord. Figure 11 represents the singulartiy distribution.

In short, this method consists in the determination of the induced velocities in a generic control point caused by vortex with unitary intensity. Running the calculations for all vortex generates a influence coefficient matrix named w.

Figure 11 – Horseshoe vortex surface discretization.

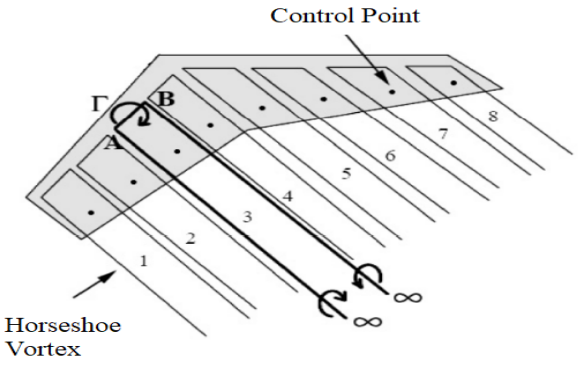

Source: Vargas (2006).

The induced velocity, in P, by a linear vortex segment named GH is given by the Equation 3.8 and this phenomena is represented by Figure 12, from the Equation 3.7.

$$\vec{V}_{ind,GH} = \frac{\Gamma}{4\pi}\frac{\vec{r_1}x\vec{r_2}}{|\vec{r_1}x\vec{r_2}|^2}\vec{r_0}\left(\frac{\vec{r_1}}{|\vec{r_1}|} - \frac{\vec{r_2}}{|\vec{r_2}|}\right) \tag{3.8}$$

Figure 12 – Induced Velocity by a vortex linear segment GH.

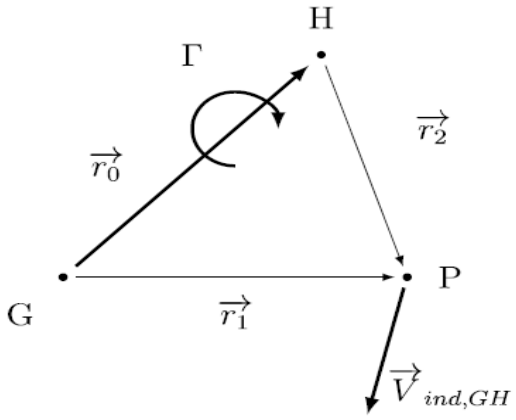

Source: Vargas (2006).

It's necessary to solve the linear system 3.9 to ensure the control points tangency. In this equation w_{ij} it's the geometric influence coefficients of the vortex induced velocity j in the point i, and can be calculated by Equation 3.10; Γ_j is the vortex intensity and B_i is the undisturbed flow velocity, given by Equation 3.11.

$$\begin{bmatrix} w_{11} & w_{12} & \cdots & w_{1n} \\ \cdots & \cdots & \cdots & \cdots \\ w_{m1} & w_{m2} & \cdots & w_{mn} \end{bmatrix} x \begin{bmatrix} \Gamma_1 \\ \Gamma_2 \\ \cdots \\ \Gamma_n \end{bmatrix} = \begin{bmatrix} B_1 \\ B_2 \\ \cdots \\ B_n \end{bmatrix}, \tag{3.9}$$

where:

$$w_{ij} = \sum_{k=1}^{n_{seg}} \vec{V}_{ijk}.\vec{n_i} \tag{3.10}$$

N_{seg} is the number of vortex segment and $\vec{V}_{ijk}$ is the induced velocity of the k segment of the vortex j in the panel i.

$$B_i = (\vec{V}_\infty + \vec{V}_m).\vec{n_i}, \tag{3.11}$$

where:

$$\vec{V}_\infty = V_\infty[cos(\alpha)cos(\beta)i - cos(\alpha)sen(\beta)j + sen(\alpha)k], \tag{3.12}$$

and:

$$\vec{V}_m = \vec{r}_{3/4}x\vec{\Omega}. \tag{3.13}$$

In Equation 3.12, α and are the angle of the attack and the sideslip angle, respectively, and $\vec{V}_\infty$ is the undisturbed velocity module. Also, $\vec{\Omega} = [pqr]$ are the maneuver angular velocity components and $\vec{r}_{3/4}$ is the distance between the control point and the aircraft rotation center.

Along this, using the Kutta-Joukowski theorem, the Equation 3.14 is obtained and using the Γ intensities, that were calculated by solving the linear system, the aerodynamic forces can now be determined.

$$\vec{F} = \rho\vec{V}_{1/4}x\vec{\Gamma}, \tag{3.14}$$

where ρ is the fluid density and $\vec{V}_{1/4}$ is the total velocity in $1/4$ of the chord. With Γ it is also possible to calculate the lift coefficient along the wingspan (c_l), using the local chord ($c(y)$), as given by the equation 3.15. Is also possible to determine the Lift Coefficient and Induced Drag Coefficient, using the Equations 3.16 and 3.17.

$$c_l(y) = \frac{2\Gamma(y)}{V_{(y)}}. \tag{3.15}$$

$$C_L(y) = \frac{1}{S}\int_{-b/2}^{b/2} c(y)c_l(y)dy \tag{3.16}$$

$$C_{D_i}(y) = \frac{2}{V_\infty S}\int_{-b/2}^{b/2} \Gamma(y)\alpha_i(y)dy. \tag{3.17}$$

3.2.4 Viscous Effects and Other Coefficients

Since the linear method hasn't discretized along the chord and hasn't take credit of the viscous effects, an adaptation, using the decambering method, is proposed.

This method consists in nine steps.

1. The auxiliary variables $\delta^i(y)$ and $\Delta c_l(y)$ assumes null values, The labels consists of sequential numbers;

2. The auxilary variable $\alpha_{decamb}(y)$ assumes the angle of attack values for the undisturbed flow (α_∞);

$$\alpha_{decamb}(y) = \alpha_\infty \tag{3.18}$$

3. $c_{l,invisc}(y)$ is determined by the lienar method using the $\alpha_{decamb}(y)$ angle;

4. Calculates the effective angle of attack ($\alpha_{eff}(y)$) using $\delta^i(y)$ as a correction variable;

$$\alpha_{eff}(y) = \frac{c_{l,invisc}(y)}{2\pi} - \delta^i(y). \tag{3.19}$$

5. By the bidimensional polar ($c_{l,2D}$) is determined $c_{l,visc}(y)$ for the $\alpha_{eff}(y)$ angles:

$$c_{l,visc}(y) = c_{l,2D}(y)(\alpha_{eff}(y)) \tag{3.20}$$

6. Calculates $\Delta c_l(y)$ for each panel:

$$\Delta c_l(y) = c_{l,visc}(y) - c_{l,invisc}(y) \tag{3.21}$$

7. Updates $\delta^i(y)$ value:

$$\delta^i(y) = \delta^{i-1}(y) + \frac{\Delta c_l(y)}{2\pi} \tag{3.22}$$

8. $\delta^i(y)$ is added to α_{decamb}:

$$\alpha_{decamb}(y) = \alpha_\infty + \delta^i(y) \tag{3.23}$$

9. Returns to the step three and starts a iterative process. The convergence criteria can be the tolerance between two values of $\Delta c_l(y)$.

Once the iterative process is over, the induced angle of attack is determinated:

$$\alpha_{ind}(y) = (\alpha_\infty + i_w(y)) - \alpha_{eff}(y) \tag{3.24}$$

These angles are represented in the Figure 13

Figure 13 – Angles of attack for a undisturbed flow

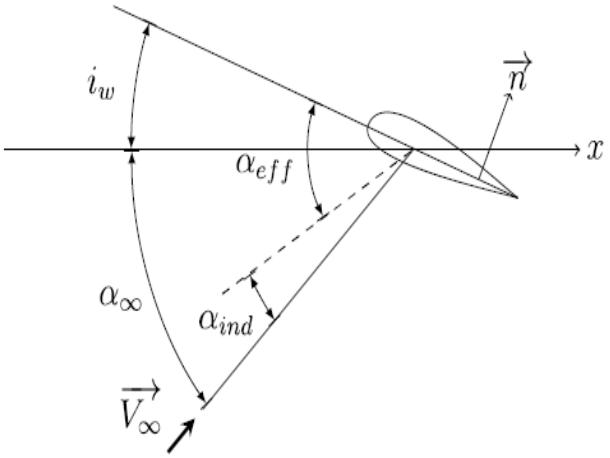

Source: Carvalho *et al.* (2018).

Using the effective angle of attack from Equation 3.20 it is possible to determine the momentum coefficient (C_m), the wing parasite drag coefficient ($C_{D,0}$), roll (C_l), induced yaw ($C_{n,i}$) and parasite yaw ($C_{n,0}$), as follows:

$$C_{D,0}(y) = \frac{1}{S}\int_{-b/2}^{b/2} c_{d,0}(y)c(y)dy. \tag{3.25}$$

$$C_m(y) = \frac{1}{Sc'}\int_{-b/2}^{b/2} c_m(y)c(y)^2dy. \tag{3.26}$$

$$C_l(y) = -\frac{1}{Sb}\int_{-b/2}^{b/2} c_l(y)c(y)ydy. \tag{3.27}$$

$$C_{n,i}(y) = \frac{1}{Sb}\int_{-b/2}^{b/2} \frac{\pi c_l(y)c(y)\alpha_i(y)}{180}ydy. \tag{3.28}$$

$$C_{n,0}(y) = \frac{1}{Sb}\int_{-b/2}^{b/2} c_{d,0}(y)c(y)ydy. \tag{3.29}$$

3.3 Structures

The structures box adopts an analytical sizing approach that allows the estimation of the wing structural weight and the aircraft empty weight. The method for the wing estimation, as

proposed by GIL A. A.; GUIMARAES, is able to generate more reliable results when compared with statistical methods traditionally used. Since this method don't relies on historical databases, it is also a good option for innovative designs.

Given the highly complex of the wing structure for the application of analytical equations, simplifications were made to make the sizing process more viable. Thus, the structural idealization method proposed by MEGSON was used in order to idealize a real wing structure by transforming it into a simpler mechanical model with equivalent mechanical properties.

Furthermore, a sizing optimization routine was proposed with the objective of finding the optimum thickness for each structural element that minimizes the wing final weight. Consequently, the output of the structural sizing box will be the lowest wing structure weight admissible for the geometry and aerodynamic load inputs provided by the multidisciplinary optimization. In addition, an estimate of the aircraft empty weight is performed here using the methodology defined by NICOLAI; CARICHNER.

3.3.1 Methods

3.3.1.1 Structural Idealization

The wing structure can be idealized into a simpler mechanical model, which has mechanical properties equivalent to the real structure. Therefore, MEGSON method was applied to replace the wing structural elements by concentrated zones known as booms. Then, a skin panel with a finite thickness is idealized as an infinitesimal thin plate with two finite booms in each row.

Since the normal forces in the real and idealized panels must be the same, the Equation 3.30 of balance of forces is used for the boom 1.

$$\sigma_2 t_D \frac{b^2}{2} + \frac{1}{3}(\sigma_1 - \sigma_2) t_D b^2 = \sigma_1 B_1 \tag{3.30}$$

where t_D is the thickness of the real panel, b is the panel length, and σ_1 and σ_2 are the normal stresses on booms 1 and 2, respectively.

On the other hand, the values of σ_1 and σ_2 are not known, so MEGSON assumes their values as the vertical distance between the boom and the section's centroid, i.e., the factors are approximated by the heights of the boom in the wing section as z_1 and z_2.

With the rearrangement of Equation 3.30, the boom 1 area can be calculated by Equation 3.31 and with Equation 3.32 the boom 2 area.

$$B_1 = \frac{t_D b}{6}(2 + \frac{z_2}{z_1}) \tag{3.31}$$

$$B_2 = \frac{t_D b}{6}(2 + \frac{z_1}{z_2}) \tag{3.32}$$

Moreover, the booms positions depend on considerations adopted by the designer. RIVELLO suggests positioning them at the central portion of each skin panel and the joint point between spars and skin panels. In this way, the spars will withstand most of normal stresses, while the skin panels will withstand most of shear stresses. In the case that there is a stiffener positioned between two booms, its cross-sectional area is added to the equations. Figure 14 shows the method proposed in the literature.

Figure 14 – Wing cross-section idealization.

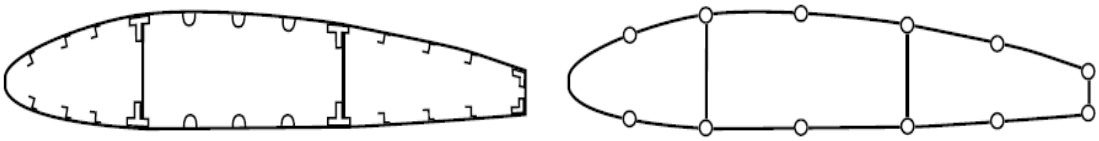

(a) Real wing cross-section (b) Idealized wing cross-section

Source: Rivello (1969).

3.3.1.2 Normal Stress and Shear Flow

After the structure idealization was performed, the previously unknown normal stresses acting on the booms can be calculated using the shear force and bending moment distributions. Equation 3.33 shows the normal stress calculation in a boom i.

$$\sigma_{yi} = -(\frac{M_z I_{xx} + M_x I_{xz}}{I_{xx} I_{zz} - I_{xz}^2})x_i + (\frac{M_x I_{zz} + M_z I_{xz}}{I_{xx} I_{zz} - I_{xz}^2})z_i, \tag{3.33}$$

where x_i and z_i are the boom i coordinates in relation to the section's centroid. In this study, only M_z values are considered, i.e. only the forces generated by the lift were estimated.

The sections along the wingspan, commonly, are not constant due to the effect of variable geometry (torsion, swept angle, and taper ratio), this variations generates stresses in the x and z direction, which must be taken into account. The components σ_x and σ_z are calculated using Equations 3.34 and 3.35, respectively.

$$\sigma_{xi} = \sigma_{yi}\frac{\delta x_i}{\delta y_i} \tag{3.34}$$

$$\sigma_{zi} = \sigma_{yi}\frac{\delta z_i}{\delta y_i} \tag{3.35}$$

where δx_i and δz_i are the variation of the position of a boom i along a span variation δy_i in the x and z directions, respectively.

For the shear flow calculation there is three steps. Initially, a pure shear flow is calculated using the shear stresses previously estimated by the aerodynamics calculations. Next, a shear flow in pure torsion is calculated using the torsional moment generated by the arm between the center of pressure, where the load is applied, and the shear center. Finally, the pure shear and pure torsion flows are summed to find the total shear flow. For each boom, the shear flow in pure shear is given by Equation 3.36 and the shear flow in pure torsion by Equation 3.37.

$$\tau_{bi} = -(\frac{S_x I_{xx} + S_z I_{xz}}{I_{xx} I_{zz} - I_{xz}^2}) x_i B_i + (\frac{S_z I_{zz} + S_x I_{xz}}{I_{xx} I_{zz} - I_{xz}^2}) z_i B_i \tag{3.36}$$

where x_i and z_i are the boom i coordinates, S_X and S_Z are shear forces in the x and z directions, respectively. As in the normal stress, only the S_Z values are considered.

$$\tau_{bi} = \frac{2 A_i G_i (\frac{d\theta}{dy}_i)}{\oint_i \frac{ds}{t}} \tag{3.37}$$

where A_i is the area of each section's cell (region between spars), G_i is the shear modulus, t is the structural element thickness as a function of its length variation ds, and $d\theta$ is the torsion angle per d unit length induced by the torsional torque.

3.3.2 Sizing Criteria

3.3.2.1 Limit Stress Criteria

In possession of the components' normal and shear stresses, they can be compared with the limit stresses of their respective materials.

The allowable limit stress is defined verifying the minimum value between the yield limit σ_{yield} and ultimate limit $\sigma_{ultimate}$ and their respective factor of safety $F_o S_{yield}$ and $F_o S_{ultimate}$ by Equation 3.38 relationship.

$$\sigma_{max} = min[(\frac{\sigma_{yield}}{F_o S_{yield}}), (\frac{\sigma_{ultimate}}{F_o S_{ultimate}})] \tag{3.38}$$

As the structural elements are subjected to normal and shear stresses at the same time, the Von Mises criterion for limit load is applied. This method is able to calculate a σ_{VM} stress equivalent to the stress tensor applied to each element. Equation 3.39 presents the Von Mises criterion by considering the stresses in the Cartesian plane used in this study.

$$\sigma_{VM} = \sqrt{\frac{(\sigma_x - \sigma_y)^2 + (\sigma_y - \sigma_z)^2 + (\sigma_x - \sigma_z)^2 + 6(\tau_{xy}^2 + \tau_{yz}^2 + \tau_{xz}^2)}{2}} \tag{3.39}$$

The stresses coefficients indicate the position in the Cartesian plane that these stresses are applied.

The Von Mises criterion will be verified in all structural elements (spars, skin panels, stiffeners, and ribs). For better results quantification, Equation 3.40 represents a margin of safety MS_{VM} which is defined by the ratio between the Von Mises stress (σ_{VM}) and the specified limit stress (σ_{max}). In other words, the MS_{VM} value must be always greater than 0.

$$MS_{VM} = \frac{\sigma_{VM} - \sigma max}{\sigma_{max}} > 0 \tag{3.40}$$

3.3.2.2 Stability Criteria

Stability criteria include failure conditions that can occur at stresses lower than the previously σ_{max} limit, caused by compressive and shear stresses in the form of buckling and crippling.

The methods used in this study to calculate instabilities in wing structures are those proposed by GERARD; BECKER. According to the literature, Equations 3.41 and 3.42 are used for calculating the critical stress in compression and shear loads, respectively. This method is used to evaluate the stability of panel elements (skin panels, spar webs and ribs).

$$\sigma_{C_{CR}} = \frac{\eta K_C \pi^2 E}{12(1-\nu_e^2)}(\frac{t}{b})^2 \tag{3.41}$$

$$\tau_{S_{CR}} = \frac{\eta K_S \pi^2 E}{12(1-\nu_e^2)}(\frac{t}{b})^2 \tag{3.42}$$

where K_C is the buckling coefficient of plates subjected to compression stress, and K_S is the buckling coefficient of plates subjected to shear stress.

The coefficients K_C and K_S are estimated using the abacuses provided in the literature of GERARD; BECKER, which consider the plates' geometry and boundary conditions. The factor η represents the plasticity correction factor, if the critical stresses found are in the plastic domain, this factor must be considered, being also estimated through abacuses provided in the literature of GERARD; BECKER, which consider the yield strength and terms that represent the shape of the stress-strain curve of the material.

Equally, the margin of safety is evaluated for a better results understanding. In that case, it calculates the ratio between the critical stresses and the real applied stresses. If the value is less than 0, there is a condition of instability. In a wing design, the buckling is not tolerated, as this may lead to a local change in the aerodynamic profile, so the margin of safety must be always greater than the specified value. Equation 3.43 shows the margin of safety in a compression condition and Equation 3.44 in a shear condition.

$$MS_C = \frac{\sigma_C - \sigma_{C_{CR}}}{\sigma_{C_{CR}}} > 0 \tag{3.43}$$

$$MS_S = \frac{\tau_S - \tau_{S_{CR}}}{\tau_{S_{CR}}} > 0 \tag{3.44}$$

The panels are also designed to work under combined compressive and shear loads, so the combined stress theory of SCHILDCROUT; STEIN can be applied by Equation 3.45.

$$(MS_C + 1) + (MS_S + 1)^2 > 1 \tag{3.45}$$

For beam elements (stiffeners and spar caps) the Gerard and Becker (1957) literature proposes the calculation of the crippling critical stress, given by Equation 3.46.

$$\sigma_{R_{CR}} = \alpha \sigma_{CY} [(\frac{t^2}{A})(\frac{E}{\sigma_{CY}})^{\frac{1}{3}}]^{\beta} \tag{3.46}$$

where σ_{CY} is the yield stress of the material and the numerical factors α and β depend on the beam geometry.

In the same way as before, the crippling critical stress is compared with the actual load applied on the element, generating the margin of safety value, given by Equation 3.47.

$$MS_R = \frac{\sigma_C - \sigma_{R_{CR}}}{\sigma_{R_{CR}}} > 0 \tag{3.47}$$

3.3.3 Optimization

The theories presented up to this point are able to verify whether a structural element is capable or not to withstand the aerodynamic loads. Conversely, this analysis requires a predetermined architecture, where the components' thicknesses are known. To solve this issue, an optimization routine was implemented with the objective of finding a configuration that minimizes the wing final weight, estimating the optimum thickness for each structural element.

Having the flight conditions, overall geometrical dimensions of the wing and the estimated lift coefficient coming from the other boxes from the MDO, becomes possible to calculate the shear forces and bending moments. Then the optimization algorithm based in the differential evolution method is launched.

In order to facilitate the convergence, the wing is divided into sections delimited by the ribs and the optimization is done individually for each section. The sizing criteria presented are evaluated and the margin of safety for each criterion can be verified.

The differential evolution algorithm uses the stop condition of the maximum number of generations. Once all the sections are designed, the wing total weight is calculated and the thicknesses values are presented to the user.

Figure 15 presents the calculation routine of the structure box.

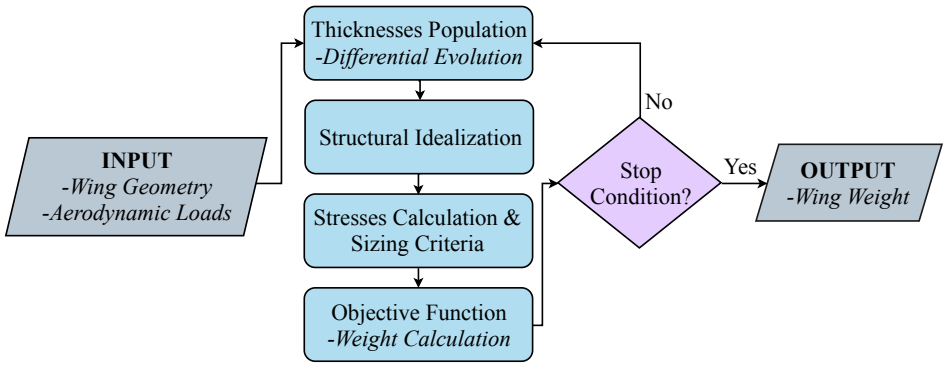

Figure 15 – Structure box flowchart.

Source: SILVA *et al.* (2019).

3.4 Flight Mechanics

The Flight Mechanics box will be responsible for the tail and control surfaces design. It is based on an analytical procedure with minimal dependence on historical data. The main constrains will come from the type of mission that the aircraft is meant to accomplish and the desired stability characteristics. Since this is an early design procedure, few geometrical data are available and, therefore, simplifications had to be applied.

The implemented methodology to size both the aircraft tail and its elevator is adapted from the one proposed by (RESENDE *et al.*, 2019). Based on the fuselage length and the wing position, it is possible to estimate the horizontal tail position. Then, the horizontal and vertical tails areas are evaluated, followed by their other geometric parameters. These evaluations are based on the wing aerodynamic data, provided by the Aerodynamic package, and on desirable characteristics for the aircraft's behavior in flight.

Since the ailerons and rudder would not play a significant contribution to the aircraft weight, their design are not considered during this MDO process in order to improve computational performance.

3.4.1 Static Stability Theory

3.4.1.1 Longitudinal Forces, Moments and Control

Lift and drag forces and the pitching moment are the main efforts presented in the longitudinal motion of an airplane. One can combine the wing and horizontal tail contributions to compute the resultant force and moment acting in the airplane's CG (Build-up method).

The wing and tail contribution to the longitudinal aerodynamic forces are very similar and can be computed by decomposing its lift and drag forces from the Wind Coordinate System to the Body Coordinate System.

The sum of the moments, due to the wing, about the CG leads to Equation 3.48 for the

Figure 16 – Flight Mechanics box flowchart.

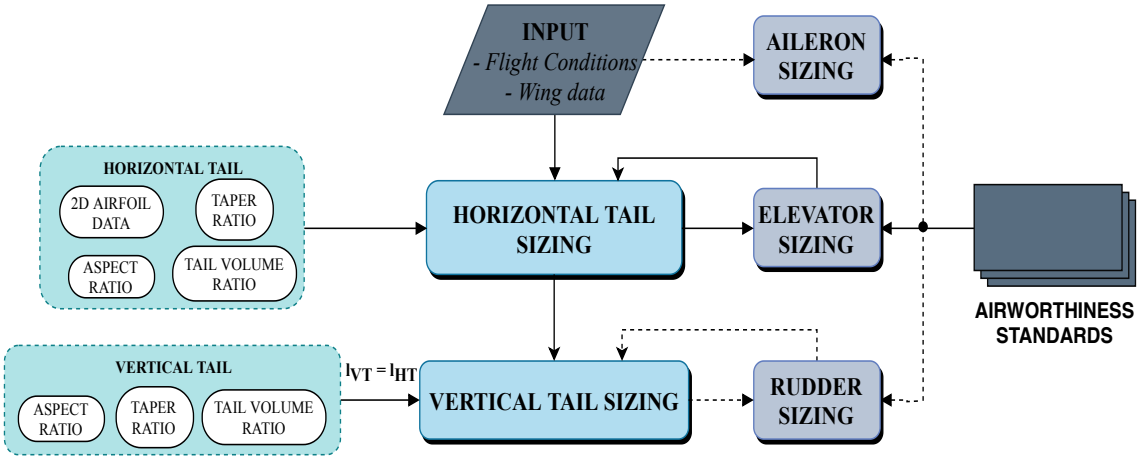

Source: SILVA *et al.* (2019).

pitching moment coefficient.

$$(C_m)_w = \frac{(h - h_{AC_w})}{\bar{c}_w} C_{L_w} - C_{m_{AC_w}} \tag{3.48}$$

The difference between the wing and tail is that the tail is experiencing a flow deviation made by the wing, which induces a downwash velocity at the air stream that implies a reduction of the horizontal tail's effective angle of attack (α_{HT}) by a downwash angle (ε). Being the horizontal tail angle of attack given by Equation 3.50:

$$\alpha_{HT} = (1 - \varepsilon_\alpha)\alpha + i_{HT} - \varepsilon_0 - \varepsilon_\alpha i_w \tag{3.49}$$

In addition, the effects of the engine's position with respect to the tail may changes the tail's dynamic pressure. The ratio between the wing and the tail aerodynamic pressure is given by:

$$\eta_{HT} = \frac{q_{HT}}{q_w} = \frac{\frac{1}{2}\rho_{HT} V_{HT}^2}{\frac{1}{2}\rho_\infty V_\infty^2} \tag{3.50}$$

The total lift acting in the CG generated by the horizontal tail is given by:

$$(C_L)_{HT} = \eta_{HT} \frac{S_{HT}}{S_w} [C_{L_{0_{HT}}} + C_{L_{\alpha_{HT}}} ((1 - \varepsilon_\alpha)\alpha + i_{HT} - \varepsilon_0 - \varepsilon_\alpha i_w)] \tag{3.51}$$

The sum of the moments about the CG, due to the aerodynamic effort acting in the tail, leads to the following equation for the pitching moment coefficient:

$$(C_m)_{HT} = -\eta_{HT} (\overline{V}_{HT} - (h - h_{AC_w}) \frac{S_{HT}}{S_w}) C_{L_{HT}} - \eta_{HT} \frac{\bar{c}_{HT} S_{HT}}{\bar{c}_w S_w} C_{m_{AC_{HT}}} \tag{3.52}$$

Futhermore, considering the wing and the horizontal tail, the total lift of the aircraft is:

$$C_L = C_{L_0} + C_{L_\alpha}\alpha, \tag{3.53}$$

where

$$C_{L_0} = (C_{L_{0_w}} + C_{L_{\alpha_w}} i_w) + \eta_{HT}\frac{S_{HT}}{S_w}[C_{L_{0_{HT}}} + C_{L_{\alpha_{HT}}}(i_H - \varepsilon_0 - \varepsilon_\alpha i_w)] \tag{3.54}$$

$$C_{L_\alpha} = C_{L_\alpha} + \eta_{HT}\frac{S_{HT}}{S_w}C_{L_{\alpha_{HT}}}(1-\varepsilon_\alpha) \tag{3.55}$$

Similarly, for the pitching moment in the airplane's CG:

$$C_m = (C_m)_w + (C_m)_{HT} \tag{3.56}$$

where

$$C_{m_0} = (h - h_{AC_w})C_{L_0} - \eta_{HT}\overline{V}_{HT}[C_{L_{0_{HT}}} + C_{L_{\alpha_{HT}}}(i_{HT} - \varepsilon_0 - \varepsilon_\alpha i_w)] - (C_{m_{AC_w}} + \eta_{HT}\frac{\overline{c}_{HT}S_{HT}}{\overline{c}_w S_w}) \tag{3.57}$$

$$C_{m_\alpha} = (h - h_{AC_w})C_{L_\alpha} - \eta_{HT}\overline{V}_{HT}C_{L_{\alpha_{HT}}}(1-\varepsilon_\alpha) \tag{3.58}$$

Notice that, from Equation 3.58, C_{m_α} depends on the CG location (h). The limit of static stability of an airplane is when the C_{m_α} approaches to zero, where it will be in a neutral equilibrium. The CG position that makes $C_{m_\alpha} = 0$ is called neutral point (h_N).

$$h_N = h_{AC_w} + \eta_{HT}\overline{V}_{HT}\frac{C_{L_{\alpha_{HT}}}}{C_{L_\alpha}}(1-\varepsilon_\alpha) \tag{3.59}$$

Longitudinal control of an airplane can be achieved, mainly, by providing an incremental lift force on the horizontal tail6. The incremental lift force can be produced by a deflection of an all move tail or by an elevator (NELSON *et al.*, 1998). Because the control surface is located at some distance from the CG, the incremental lift force creates a moment about the airplane's CG. Hence, the total lift and moment coefficients becomes:

$$C_L = C_{L_0} + C_{L_\alpha}\alpha + C_{L_{\delta_e}}\delta_e \tag{3.60}$$

$$C_m = C_{m_0} + C_{m_\alpha}\alpha + C_{m_{\delta_e}}\delta_e \tag{3.61}$$

3.4.1.2 Latero-Directional Forces and Moments

Latero-directional stability is concerned with the static stability of the aircraft about the x and z-axis, also known as roll stability and directional stability respectively. Similarly to the case of longitudinal static stability, it is desirable that the aircraft has a tendency to return to its initial condition after a yawing perturbation or a roll perturbation.

The main contribution to directional stability comes from the vertical tail, which produces a lift-like force parallel to the *xy* plane when the aircraft is flying at sideslip. The assembly wing-fuselage has a destabilizing, although it is very small when compared to the vertical tail contribution.

So, when the aircraft is flying with a positive sideslip angle, the angle of attack experienced by the vertical tail is given by Equation 3.62, where σ is the sidewash angle created by the wing distortion in the flow field. It is analogous to the downwash for the horizontal tail.

$$\alpha_{VT} = +\sigma \tag{3.62}$$

And the contribution of the vertical tail to roll and directional stability are given by Equations 3.63, 3.64 and 3.65.

$$C_{Y_\beta} = -\eta_{VT} C_{L_{\alpha_{VT}}} \frac{S_{VT}}{S_w}(1+\frac{d\sigma}{d\beta}) \tag{3.63}$$

$$C_{l_\beta} = \frac{-|z_{VT}|S_{VT}}{bwS_w}\eta_{VT} C_{L_{\alpha_{VT}}}(1+\frac{d\sigma}{d\beta}) \tag{3.64}$$

$$C_{n_\beta} = V_{VT}\eta_{VT} C_{L_{\alpha_{VT}}}(1+\frac{d\sigma}{d\beta}) \tag{3.65}$$

3.4.2 Tail and Control Surfaces Sizing

3.4.2.1 Horizontal Tail and Elevator

From Equations 3.55 to 3.59, the design of horizontal tail can be accomplished and the only unknown variable is the horizontal tail surface. Hence, substituting the C_{L_α} equation into the neutral point equation, one may obtain:

$$S_{HT} = \frac{S_w}{\eta_{HT} C_{L_{\alpha_{HT}}}(1-\varepsilon_\alpha)}[\frac{\eta_{HT}\overline{V}_{HT} C_{L_{\alpha_{HT}}}(1-\varepsilon_\alpha)}{h_n - h_{AC_w}} - C_{L_{\alpha_w}}] \tag{3.66}$$

h_n is usually an imposed parameter, since the minimal statical stability margin and the most forward CG position are given. Also, from Equation 3.66 is noticed that $\overline{V}_{HT}$ is a paramter that

depends on S_{HT}, so it is necessary to perform a parametric evaluation of the tail volume ratio before determine the tail surface area.

$$\overline{V}_{HT} > (\overline{V}_{HT})_{critical} = C_{L_{\alpha_w}} \frac{(h_n - h_{AC_w})}{\eta_{HT} C_{L_{\alpha_{HT}}} (1 - \varepsilon_\alpha)} \tag{3.67}$$

The elevator sizing is based on guarantee that the aircraft will be able to be in a trim condition at critical flight conditions (e.g. at the stall velocity, for a longitudinal trim).

At this point, the elevator dimensions and its effectiveness parameter (τ) is unknown. However, with Equations 3.60 and 3.61 becomes possible to create the linear system 3.68 to determinate τ and the elevator surface (S_e) by using Figure 17.

$$\begin{bmatrix} C_{L_\alpha} & \eta_{HT} \frac{S_{HT}}{S_W} C_{L_{HT}} \delta_{e_{min}} \\ C_{m_\alpha} & -\eta_{HT} \overline{V}_{HT} C_{L_{HT}} \delta_{e_{min}} \end{bmatrix} \begin{Bmatrix} \alpha \\ \tau \end{Bmatrix} = \begin{Bmatrix} C_{L_{@V_{stall}}} - C_{L_0} \\ -C_{m_0} \end{Bmatrix} \tag{3.68}$$

Figure 17 – Flap effectiveness parameter.

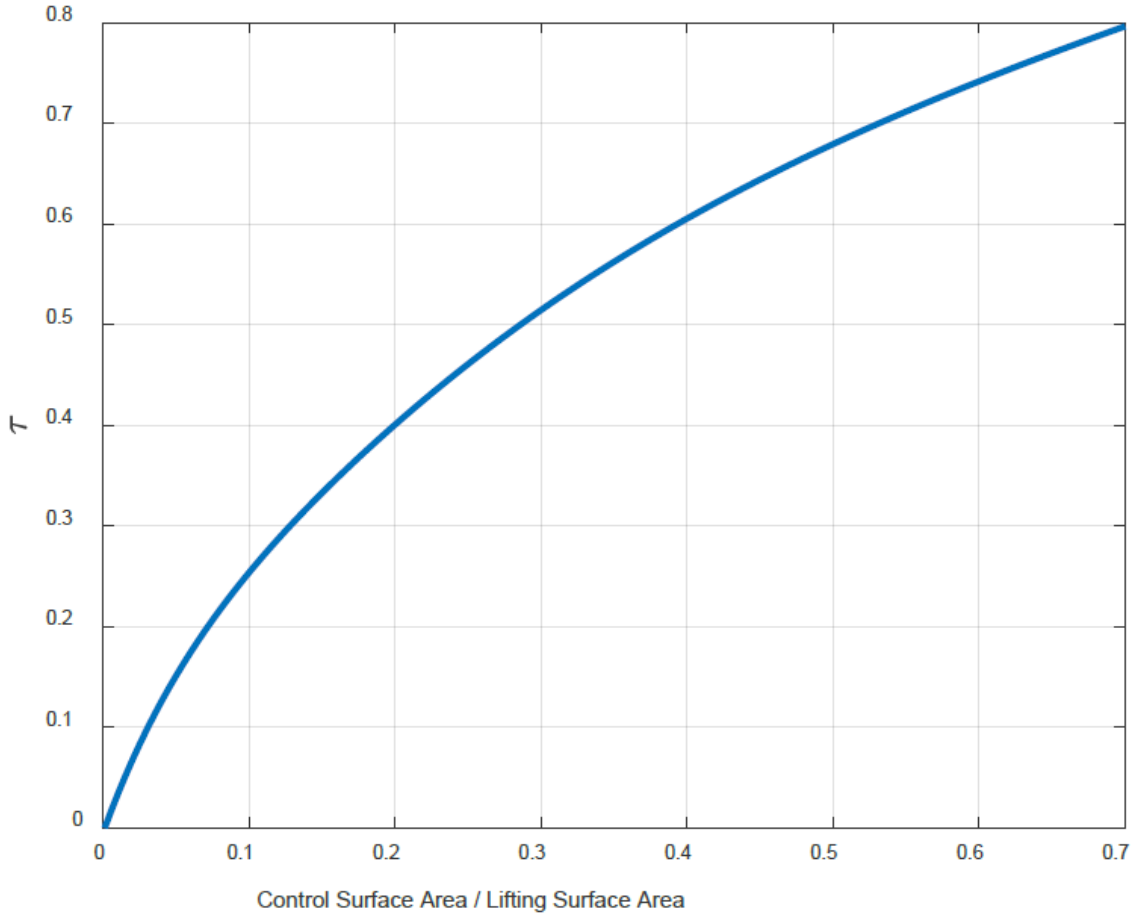

Source: Resende *et al.* (2019).

3.4.2.2 Vertical Tail

The assumption that both vertical and horizontal tails has their aerodynamic center aligned, is not a strong one for conventional configuration (Gudmundsson, 2014). Hence, with l_{VT} determined, the vertical tail surface is:

$$S_{VT} = \frac{V_{VT} b_w S_w}{l_{VT}} \tag{3.69}$$

The choice of the vertical tail volume ratio (V_{VT}) is such that, there will be enough area for the rudder on the vertical tail, so the lateral stability requirements can be fulfilled.

As said before, since the ailerons and rudder don't play a significant contribution to the aircraft weight, their design are not considered during this MDO process in order to improve computational performance.

3.5 Mission

The mission box is responsible to evaluate a typical mission of the aircraft. From operational requirements, the box evaluates the powertrain necessary to meet constraints of takeoff, climb, cruise, climb, descent, loiter, and approach. In this process, it is computed the required power for each flight phase, and then it is estimated the corresponding weight of electric motors and engines as described by SILVA *et al.*. Also, for a certain combination of degree-of-hybridization throughout the typical mission, the energy supplied by the batteries is estimated, and, consequently, its weight.

Finally, the box estimates the weight breakdown of the aircraft, i.e., the empty weight, payload, powertrain weight, and the fuel consumption during the mission. The MDO may be set to find the best configuration of the aircraft that results in lower fuel consumption, for example. Other objective function in terms of performance could be to carry more payload, and so on. Figure 18 presents the calculation routine of the structure box.

Figure 18 – Overlay procedure flowchart

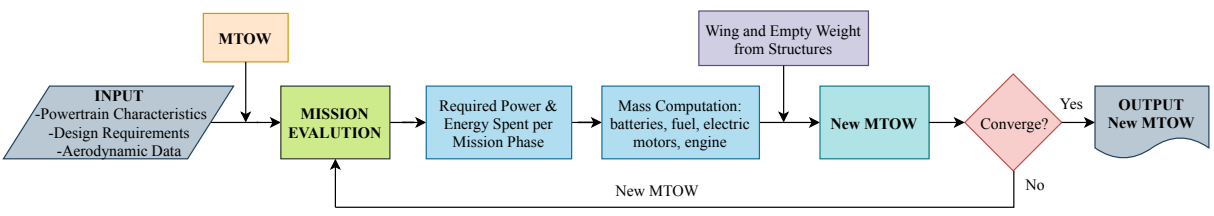

Source: SILVA *et al.* (2019).

3.5.1 Power Constraints

Since its a hybrid-electric aircraft design it's necessary to define the supplied power ratio, that defines the amount of power drawn from the electrical energy source with respect of the total energy drowned (battery and fuel).

$$\Phi = \frac{P_{bat}}{P_{bat} + P_f} \tag{3.70}$$

where P_{bat} is the power from the battery and P_f from the fuel.

The second parameter to be defined is the shaft power ratio, that represents the amount of shaft power produced by the electrical machines with respect to the total amount of shaft power produced, defined as:

$$\varphi = \frac{P_{s2}}{P_{s1} + P_{s2}} \tag{3.71}$$

Also, the gas turbine throttle, which represents the power produced by the gas turbine with respect to the maximum power it can produce in the given flight condition.

$$_{GT} = \frac{P_{GT}}{P_{GT,max}} \tag{3.72}$$

There is also a correction of the altitude lapse, presented below, that assumes the engine power is directly dependent on the density ratio:

$$P = P_{SL}\frac{\rho}{\rho_{SL}} \tag{3.73}$$

where P_{SL} and ρ_{SL} correspond to sea-level values.

At last, knowing the architecture applied to the design, from the ones presented in 4, it's necessary to evaluate the components that are part of the chosen architecture and each efficiency associated through a power balance of each generic component.

$$\sum P_{out} = \eta_i \sum P_{in} \tag{3.74}$$

where the left-hand side are the powers that leave each component and the right-hand side is the powers that enter the components multiplied by the efficiencies of the components.

3.5.1.1 Wing and Powertrain Sizing

In conventional aircraft designs, propulsive effects are not taken into account in aerodynamic calculations (lift and drag). In other words, the sizing methods are simplified. However, when having configurations with distributed propulsion, it is important to take into account these

effects, since they directly modify the aerodynamic flow throughout the aircraft, which results in different lift and drag components. Nonetheless, the DP contributes directly to the thrust.

The total thrust of the aircraft (T) is the sum of thrust components from the different propulsive systems. T_0 two fans installed on the wing and T_{dp} for the component produced by the array of distributed propulsors installed over the wing, which presents strong interaction effects with the airframe that can also be expressed by component efficiencies. Thus,

$$T = T_0 + T_{dp} \tag{3.75}$$

$$\eta_{dp} = \eta_{dp,isolated} + \Delta\eta_{dp}(T_{dp}, L_{airframe}, S, ...) \tag{3.76}$$

where $\eta_{dp,isolated}$ is the propulsive efficiency of these propulsors and $\Delta\eta_{dp}$ is the change in propulsive efficiency when installed on the aircraft due to its interaction with the airframe.

The total lift and drag produced by the aircraft can be expressed by its coefficients on Equations 3.77 and 3.78, respectively.

$$C_L = C_{L_{airframe}} + \Delta C_L(T_{dp}, C_{L_{airframe}}, S, ...) \tag{3.77}$$

$$C_D = C_{D_0} + \Delta C_{D_0}(T_{dp}, C_{L_{airframe}}, S, ...) + C_{D_i} + \Delta C_{D_i}(T_{dp}, C_{L_{airframe}}, S, ...) \tag{3.78}$$

Therefore, the airframe component is the ones determinated by the aerodynamic box and the aero-propulsive interaction effects of the distributed propulsors are expressed by means of these "Deltas", which are estimated using detailed aerodynamic analyses, explained SILVA *et al.*, resulting in the equations:

$$\Delta c_L = 2\pi[(sin\alpha - a_{c/4}sin(i_p))\sqrt{(a_{c/4})^2 + 2a_{c/4}cos(\alpha + i_p) + 1} - sin\alpha] \tag{3.79}$$

where α is the geometric angle of attack of the wing, i_p is the angle between the propeller axis and the wing chord, $_{dp}$ is a finite-slipstream correction factor and $a_{c/4}$ is given by Equation 3.80 that is a function of the contraction ratio of the slipstream at the wing ($R_{c/4}/R_p$).

$$a_{c/4} = \frac{1 + a_p}{(R_{c/4}/R_p)^2} - 1 \tag{3.80}$$

From 3.79 it is possible to calculate the change in drag coefficient, which is split into Δc_{d_0} and Δc_{d_i}.

$$\Delta c_{d_0} = a_{c/4}^2 c_f \tag{3.81}$$

$$\Delta c_{d_i} = \frac{2C_{L_{airframe}}\Delta c_l}{\pi AR} \tag{3.82}$$

where c_f is the sectional skin friction coefficient, for which a value of 0.009 is assumed, and AR is the aspect ratio.

The lift and drag coefficients calculated so far are two-dimensional coefficients and represent an average value for the DP system. So, assuming the effect of the propellers on the wing is limited to the spanwise interval they occupy, the three-dimensional coefficients can be related to the corresponding average sectional coefficients as:

$$\Delta C_L = \Delta c_l(\frac{\Delta y}{b}) \tag{3.83}$$

$$\Delta C_{D_0} = \Delta c_{d_0}(\frac{\Delta y}{b}) \tag{3.84}$$

$$\Delta C_{D_i} = \Delta c_{d_i}(\frac{\Delta y}{b}) \tag{3.85}$$

Also, for conventional aircraft, there is only the thrust component aligned to the velocity vector (T_0); however, here there is an additional component (T_{dp}), which is produced by the DP system.

Applying Newton's second law along the X, Y and Z axes represented in the Figure 19, it is possible to determine the equilibrium equations, from where is writed the total thrust-to-weight ratio of the aircraft (T/W):

$$\frac{T}{W} = \frac{\frac{q_\infty}{(W/S)}(C_{D_0} + \Delta C_{D_0} + \frac{C^2_{L_{airframe}}}{\pi eAR} + \Delta C_{D_i}) + \frac{h}{V} + \frac{1}{g}\frac{dV}{dt}}{1 - X(1 - cos\alpha_p)}, \tag{3.86}$$

Since ΔC_{D_0} and ΔC_{D_i} are functions of T/W, Equation 3.86 becomes a transcendental equation. Thus, it is necessary to couple 3.86 to another transcendental equation of W/S described in 3.87.

$$\frac{W}{S} = \frac{q_\infty cos\mu(C_{L_{airframe}} + \Delta C_L)}{\sqrt{1 - (\frac{h}{V})^2 - Xsin\alpha_p cos\mu(\frac{T}{W})}}. \tag{3.87}$$

3.5.2 Weight Breakdown

3.5.2.1 Typical Mission of a Aircraft

The typical mission of the aircraft is defining for the design. With it is possible to determinate the amount of fuel, or in hybrid-electric case, amount of energy necessary to execute

Figure 19 – DP-system representation

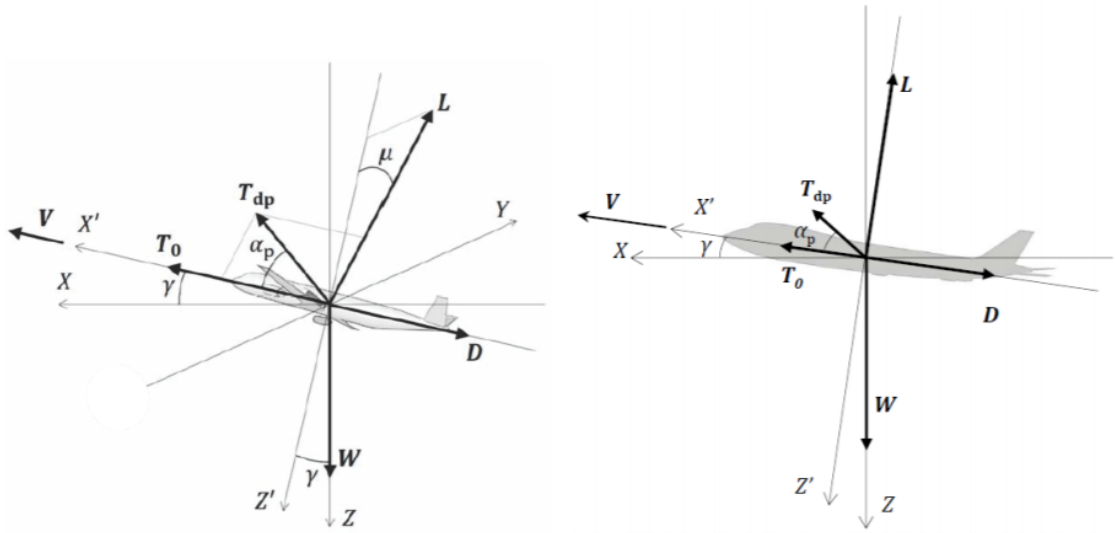

(a) Asymmetric flight. (b) Symmetric flight, $\mu = 0$.

Source: Silva *et al.* (2019).

the flight. Knowing that the fuel and batteries are going to be a considerably part of the weight, also very important for the weight breakdown. So, the typical mission profile show in Figure 20 is defined:

Figure 20 – Typical Mission Profile

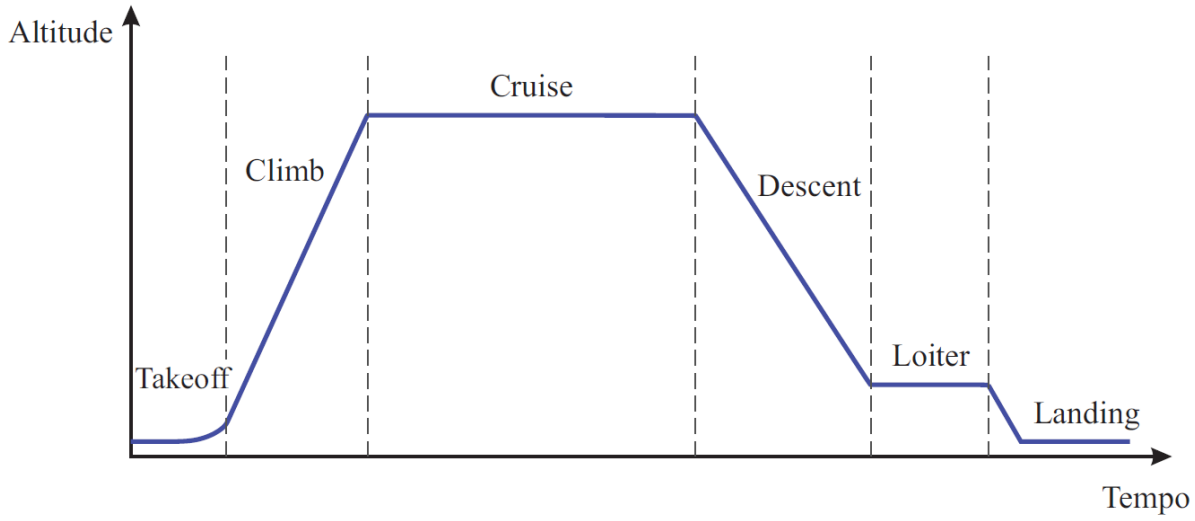

Source: Silva *et al.* (2019).

3.5.2.2 Energy Sizing

The adopted method consists in calculate the energy consumption spent in each flight phase and then, knowing the hybridisation degree of each phase, is possible to size the fuel

and/or battery weight that would be required for that mission.

Firstly, the takeoff weight can be defined as:

$$W_{TO} = W_{empty} + W_{bat} + W_{fuel} + W_{PT} + W_{PL} \tag{3.88}$$

where W_{empty} is the empty weight of the aircraft, W_{bat} the battery weight, W_{fuel} the fuel weight, W_{PT} the powertrain components weight and W_{PL} the payload weight.

The empty weight can be estimated from takeoff weight (W_TO) using statistical regression (ROSKAM, 1985), as follows:

$$log_{10}W_{TO} = A + Blog_{10}W_{empty}, \tag{3.89}$$

where A and B coefficients are taken from Table 3.

Table 3 – Statistical regression values relating empty weight to takeoff weight

Aircraft type	A	B
Homebuilt	0.3411	0.9519
Single-engine propeller driven	-0.1440	1.1162
Twin-engine propeller driven	0.1063	1.0351
Agricultural	-0.4398	1.1946
Business Jet	0.2678	0.9979
Regional turboprop	0.3874	0.9647
Transport jet	0.0833	1.0383
Military bomber, transport, patrol	-0.2009	1.1037

Source: Roskam (1985).

The payload weight (W_{PL}) can be estimated by adding the weight of the crew (including pilot) without luggage (N_{crew}) and the weight of passengers with luggage (N_{pax}), as follows:

$$W_{PL} = (N_{crew}78 + N_{pax}102)g, \tag{3.90}$$

The powertrain weight (W_{PT}) depends on the chosen architecture and the number of components and motors.

Having the aerodynamic parameters calculated by the aerodynamic box, it is possible to estimate the performance of the aircraft in each phase of the mission by estimating the power required and the elapsed time of each one. Then, it is possible to determine the energy that the aircraft requires and then calculate the fuel and batteries weight.

For the takeoff it is analysed the ground run phase and airborne one. Since it is not possible to determinate the acceleration over time, it will be necesary to take into account the distance traveled. It is given that:

$$L_{TO} = L_{GR} + L_{AB} \tag{3.91}$$

To calculate the required power during ground run (P_GR), it is necessary to find a value of P that satisfies:

$$L_{GR} = \int_0^{V_{TO}} \frac{M_{TO}V}{\frac{P}{V_{TO}} - \frac{1}{2}\rho_{TO}V^2SC_{D_{TO}} - \mu(W_{TO} - \frac{1}{2}\rho_{TO}V^2SC_{L_{TO}})}dV \tag{3.92}$$

where the takeoff speed must be greater than the stall speed.

The airborne power required is given by the Equation 3.94 and is a function of the climb angle γ.

$$P_{AB} = \frac{1}{2}\rho_{TO}V_{TO}^3SC_{D_{TO}} + W_{TO}V_{TO}sin\gamma \tag{3.93}$$

Then, the takeoff power P_{TO} is the maximum value between P_{GR} and P_{AB}.

$$P_{TO} = max[P_{GR}, P_{AB}] \tag{3.94}$$

and the takeoff time can be simply estimated considering the whole distance at takeoff speed:

$$\Delta t_{TO} = \frac{L_{TO}}{V_{TO}} \tag{3.95}$$

and the required energy for takeoff phase is obtained by multiplying the takeoff power with takeoff time:

$$E_{TO} = P_{TO}\Delta t_{TO} \tag{3.96}$$

For climb, the power is given by:

$$P_{CL} = \frac{1}{2}\rho_{CL}V_{CL}^3SC_{D_{CL}} + W_{CL}V_{v_{CL}} \tag{3.97}$$

where $V_{v_{CL}}$ is the vertical velocity (rate of climb). Moreover, the elapsed climb time is defined as the time that the aircraft takes to climb from the airport altitude ($h_{airport}$) to cruise altitude (h_{cruise}) at a certain rate of climb:

$$\Delta t_{CL} = \frac{h_{cruise} - h_{airport}}{V_{v_{CL}}} \tag{3.98}$$

And then:

$$E_{CL} = P_{CL}\Delta t_{CL} \tag{3.99}$$

and the horizontal distance traveled during climb is then calculated using average climb speed:

$$R_{CL} = V_{CL}\Delta t_{CL} \tag{3.100}$$

For the descent it takes the same procedure as the climb, but considering now the parameters for this phase and that the aircraft is going from cruise altitude (h_{cruise}) to loitter altitude ($h_{loitter}$). Then:

$$P_{DS} = \frac{1}{2}\rho_{DS}V_{DS}^3 SC_{D_{DS}} + W_{DS}V_{v_{DS}} \tag{3.101}$$

$$\Delta t_{DS} = \frac{h_{loitter} - h_{cruise}}{V_{v_{DS}}} \tag{3.102}$$

$$E_{DS} = P_{DS}\Delta t_{DS} \tag{3.103}$$

$$R_{DS} = V_{DS}\Delta t_{DS} \tag{3.104}$$

At cruise stage the required power is obtained by:

$$P_{CR} = \frac{1}{2}\rho_{CR}V_{CR}^3 SC_{D_{CR}} \tag{3.105}$$

The time depends on the cruise speed and the total distance traveled:

$$\Delta t_{DS} = \frac{R_{CR}}{V_{CR}} \tag{3.106}$$

where the R_{CR} is the remaining range after considering the one's spent in the Climb and Descent phase, so:

$$R_{CR} = R_{total} - R_{CL} - R_{DS} \tag{3.107}$$

And, finally, the energy spent during cruise phase is calculated as follows:

$$E_{CR} = P_{CR}\Delta t_{CR} \tag{3.108}$$

And the power and energy in loitter:

$$P_{LT} = \frac{1}{2}\rho_{LT} V_{LT}^3 S C_{D_{LT}} \tag{3.109}$$

$$E_{LT} = P_{LT}\Delta t_{LT} \tag{3.110}$$

where Δt_{LT} is the loitter time required and V_{LT} is the maximum value between the stall speed and the minimum required power speed, that is given by:

$$V_{mp} = \frac{1}{\sqrt{43}} V_{md}, \tag{3.111}$$

where:

$$V_{md} = \sqrt{\frac{2W_{LT}}{\rho_{LT} S}\sqrt{\frac{1}{\pi e A R C_{D_0}}}} \tag{3.112}$$

3.5.2.3 Mission Evaluation

Having all of those required power and energy spent per mission phase, it is possible to size the gas turbine, the electric motors, the batteries and the fuel. The gas turbine and the electric motors are sized for the maximum required power that occurs in some phase of the flight. Then, the maximum required power, and its phase, is thus calculated:

$$P_{max} = max[P_{TO}, P_{CL}, P_{CR}, P_{DS}, P_{LT}] \tag{3.113}$$

However, the energy required is the sum of all the energies of each phase:

$$E_{total} = E_{TO} + E_{CL} + E_{CR} + E_{DS} + E_{LT} \tag{3.114}$$

an it can also be written as

$$E_{total} = P_{TO}\Delta_{TO} + P_{CL}\Delta_{CL} + P_{CR}\Delta_{CR} + P_{DS}\Delta_{DS} + P_{LT}\Delta_{LT} \tag{3.115}$$

Considering, also, the aircraft's hybridization degree:

$$\Psi = \frac{P_{bat}}{P_{bat} + P_{gt}} \tag{3.116}$$

and each phase has it own value for Ψ.

Now, for each chosen architecture there will be a new equation of power since it takes into account the aircraft power system components. However, taking the serial architecture as an example and solving for the gas turbine power with the respective efficiencies, is obtained:

$$P_{gt,phasei} = (\frac{1}{\eta_{pm}\eta_{em2}\eta_{p2}})[\frac{1-\Psi_{phasei}}{\Psi_{phasei}+\eta_{gb}\eta_{em1}(1-\Psi_{phasei}}})]P_{phasei} \tag{3.117}$$

where Ψ_{phasei} and P_{phasei} are the correspondent degree-of-hybridization and aircraft required power in each flight phase, respectively. Therefore, the gas turbine can be sized from the flight phase that it needs to provide the maximum power. Thus,

$$P_{gt,max} = max[P_{gt,TO}, P_{gt,CL}, P_{gt,CR}, P_{gt,DS}, P_{gt,LT}] \tag{3.118}$$

Since the gas turbine is affected by the altitude and the given maximum power is obtained to the flight altitude, it is necessary to estimate the required power at sea-level using the equation 3.73. With the required power for the gas turbine, using the regression proposed by ROSKAM becomes possible to estimate its weight:

$$W_{gt} = 0.1860 P_{gt,SL} g \tag{3.119}$$

where $P_{gt,SL}$ is given in kW.

Also, by determining the power split of each phase, with the degree-of-hybridization (Ψ), is possible to calculate the battery weight, when assuming a specific energy of the batery (e_{bat} [Wh/kg]):

$$W_{bat} = \frac{\sum_{i=1}^{no\,f\,phases}(P_{bat,phasei}\Delta t_{phasei})}{e_{bat}} g \tag{3.120}$$

$$P_{bat,phasei} = (\frac{1}{\eta_{pm}\eta_{em2}\eta_{p2}})[\frac{\Psi_{phasei}}{\Psi_{phasei}+\eta_{gb}\eta_{em1}(1-\Psi_{phasei}}})]P_{phasei} \tag{3.121}$$

Regarding safety and aiming increase the battery life, the batteries are only going to be discharged until reaching the state-of-charge (SOC) of 25%. Then, the final weight battery is estimated by:

$$W_{bat} = \frac{W_{bat,old}}{1-SOC} \tag{3.122}$$

Similarly, assuming the η_{gt} which is assumed to be 0.3, the fuel weight is going to be given by:

$$W_{fuel} = \frac{\sum_{i=1}^{nofphases}(P_{fuel,phasei}\Delta t_{phasei})}{e_f}g, \tag{3.123}$$

where:

$$P_{fuel,phasei} = (\frac{1}{\eta_{gt}\eta_{pm}\eta_{em2}\eta_{p2}})[\frac{1-\Psi_{phasei}}{\Psi_{phasei}+\eta_{gb}\eta_{em1}(1-\Psi_{phasei}}})]P_{phasei} \tag{3.124}$$

Regarding safety, also, there is a fuel reserve (SOF) of 10% is usually kept. So, the new fuel weight is going to be:

$$W_{bat} = \frac{W_{bat,old}}{1-SOF} \tag{3.125}$$

For the electric motors weight is possible to estimate using historical data that generates the Equation 3.128.

$$W_{em} = (1.9309 + 0.1933\frac{P_{max}}{2N\eta_{p2}})g \tag{3.126}$$

Finally, the powertrain weight is estimated by the sum of the weight of the engine and electric motors:

$$W_{PT} = W_{gt} + 2NW_{em} \tag{3.127}$$

Furthermore, the first Empty Weight estimation takes into account historical data of aircraft with propulsive system included. So, a correction must be done so the powertrain weight be accounted only once.

$$W_{empty,new} = W_{empty,old} - W_{PT} \tag{3.128}$$

CHAPTER

4

VALIDATION

In order to validate the accuracy of the aerodynamic and flight mechanics solvers, their results were confronted with two others software: XFLR5 and OpenVSP. A base-line model, composed by a wing with $\mathcal{AR}_w = 15.0$, $\lambda_w = 0.40$ and area of 8.64 m^2 and by a horizontal tail with $\mathcal{AR}_{HT} = 5.8$, $\lambda_{HT} = 0.38$ and area of 1.39 m^2. The wing and horizontal tail airfoils were the NACA23012 and the AH21 (with inverted camber), respectively. The CG position was fixed 0.214 m from the wing leading edge, considered at its root chord, and the horizontal tail is placed 4.72 m from the same reference.

For this test case, the freestream velocity was set to 82.3 m/s and the Reynolds number to 3.8×10^6, simulating a cruise flight condition for general aviation aircraft. The aerodynamic solver evaluated this simulation as described in Section 3.2. Both the XFLR5 and OpenVSP performed a VLM calculation with similar mesh. The XFLR5, however, considered a correction model to account for viscous effects.

Figure 21 shows the aerodynamic coefficients obtained by each solver, and Tab. 4 presents their numeric values at $\alpha = 0^o$ and $\alpha = 5^o$. As expected, the lift coefficient had a good agreement between the methods. The drag coefficient, however, is more sensitive to the adopted methodology on each software. Despite of that, the differences encountered were considered to be acceptable.

From Fig. 24, it is clear that all solvers evaluated similar slopes for the pitching moment coefficient, which is a reasonable indicator that the flight mechanics package will be feed with coherent data for the tail and elevator sizing. The variation between the curves may be explained by how each software evaluates the airfoils pitching moment around their aerodynamic center, which would cause a shift in the C_{m_0} (pitching moment coefficient at $\alpha = 0^o$) of the assembly wing-horizontal tail. Furthermore, a static stability calculation was performed on each software to evaluate the assembly neutral point (X_{NP}). As shown in Tab. 5, the flight mechanics solver had good agreement with the two different software computations of the pitching moment slope

(C_{m_α}) and the X_{NP}.

Figure 21 – Aerodynamic solver validation

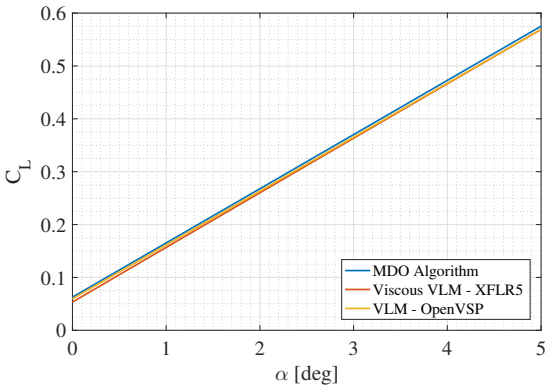

Figure 22 – C_L x α curve.

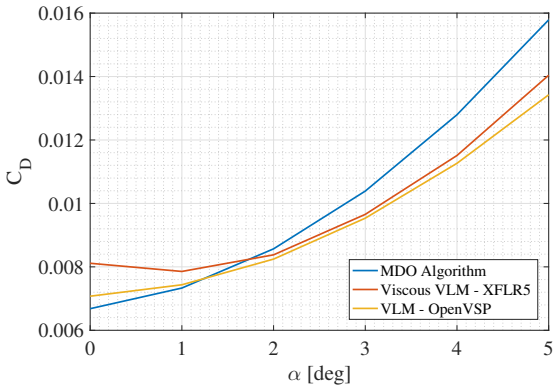

Figure 23 – C_D x α curve.

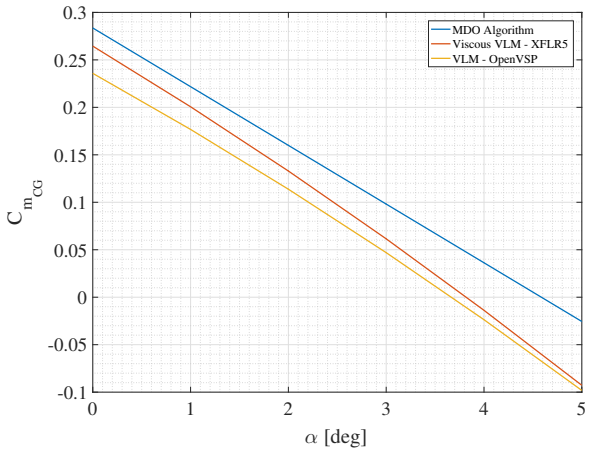

Figure 24 – $C_{m_{CG}}$ x α curve.

Table 4 – Numeric values for aerodynamic solver validation.

	MDO	XFLR5	OpenVSP	MDO	XFLR5	OpenVSP
	$\alpha = 0^o$			$\alpha = 5^o$		
C_L	0.0628	0.0533	0.0595	0.5752	0.5692	0.5692
C_D	0.0067	0.0081	0.0071	0.0158	0.0140	0.0134
$C_{m_{CG}}$	0.2836	0.2645	0.2358	-0.0256	-0.0928	-0.0982

Table 5 – Numeric values for flight mechanics solver validation.

	MDO	XFLR5	OpenVSP
X_{NP}	3.676	3.660	3.658
C_{m_α} [rad^{-1}]	-3.543	-4.094	-3.385

CHAPTER

5

CASE STUDY

It is proposed a general aviation aircraft with short range design to cover a mission of 300 km with the requirements and specifications listed in Tab. 6. Also, is established a comparison between an all-electric and a hybrid-electric aircraft, named E-4P and H-4P, respectively. The aircraft still has a distributed propulsive system along the wing and a serial powertrain architecture, as illustrated in Fig. 25, and it ends the mission with the recommended levels of battery, 25% SOC, and fuel, 10% SOF, for safety issues.

For the optimization problem, a multi-objective approach was selected and to find the Pareto solution, it is used the NSGA II, a multi-objective algorithm based on genetic algorithms and proposed by DEB *et al.*. The algorithm was executed several times with a number of populations of 100, generation equal to 500, crossover index of 20, and mutations index of 20. These parameters were also changed, but all the results converged to the same.

Figure 25 – Schematic representation of distributed propulsion along the wing and serial powertrain architecture. Legend: “F” = fuel, “GT”= gas turbine, “GB”= gearbox, “P”= propulsor, “BAT”= batteries, “EM”= electrical machine (i.e. electric motor or generator), “PM”= power management.

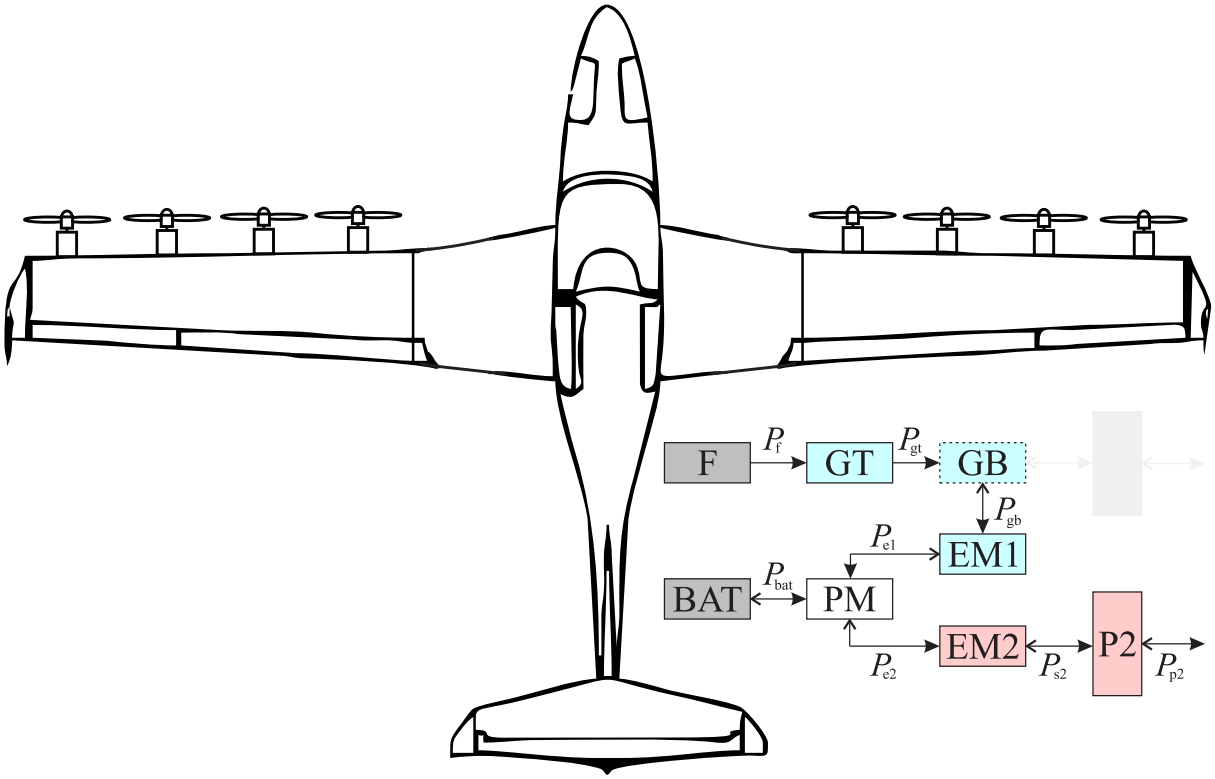

Table 6 – Design requirements and specifications

Parameter	Value	Unit
Number of passengers	3	-
Number of pilots	1	-
Number of engines	1	-
Number of electric propulsors	8	-
Stall speed	60	
Cruise speed	160	KTAS
Climb/descent speed	105	EAS
Climb rate	500	fpm
Descent rate	-350	fpm
Takeoff field length	325	m
Cruise altitude	8000	ft
Loiter altitude	1000	ft
Loiter time	45	min
Battery specific energy	500	Wh/kg
Fuel specific energy	11900	Wh/kg

As objectives of this case study, two functions are chosen to be minimized: W_{fuel} and $MTOW$. Also, the selected design variables (x) are based on values of geometry and performance,

i.e., wing profile, horizontal tail profile, wing aspect ratio ($\mathcal{AR}_w$), wing taper ratio (λ_w), horizontal tail aspect ratio ($\mathcal{AR}_{HT}$), horizontal tail root chord ($c_{\text{root},HT}$), and the degrees-of-hybridization per flight phase ($\psi_{\text{phase},i}$). Thus, the optimization problem proposed here is characterized as follows:

$$\textit{Multi-objective optimization problem} : \begin{cases} \min\left(W_{fuel}\right) \quad \text{and} \quad \min\left(W_{TO}\right) \\ x : [\text{Airfoil}_w, \text{Airfoil}_{HT}, \mathcal{AR}_w, \lambda_w, \mathcal{AR}_{HT}, c_{\text{root},HT}, \psi_{TO}, \psi_{CL}, \psi_{CR}, \psi_{DS}, \psi_{LT}] \\ \text{Airfoil}_w = \text{NACA63}_1412, \text{SELIG1223, NACA2412, NACA23012} \\ \text{Airfoil}_{HT} = \text{NACA0012, AH21, NACA63-012} \\ 7 \leq \mathcal{AR}_w \leq 15 \\ 0.40 \leq \lambda_w \leq 1.00 \\ 3 \leq \mathcal{AR}_{HT} \leq 6 \\ 0.50 \leq c_{\text{root},HT} \leq 1.00 \\ 0 \leq \psi_{\text{phase},\,i} \leq 1 \end{cases} \tag{5.1}$$

The Pareto-optimal front depicted in Fig. 26 show the solution for the optimization of the case study. The result shows that to minimize the fuel consumption for this type of mission, it is necessary to increase the amount of batteries onboard. However, due to the lower specific energy of the batteries in comparison with the fuel, as the quantity of batteries increases, the weight of the aircraft increases as a whole, i.e., the maximum takeoff weight increases as well. Therefore, to reduce the fuel weight, the total weight of the aircraft is considerably increased. Regarding the design variables, the NSGA II algorithm found different combinations that delivered that result. Among those combinations, all the wing airfoil profiles were used, but only the AH21 and NACA63-012 were selected for the horizontal tail profile. The aspect ratio remained around 14.3 to 15 for the wing and 4.2 and 5.9 for the horizontal tail. Moreover, the wing taper ratio presented values from 0.40 to 0.70 and the horizontal tail root chord varied from 0.50 to 1.00.

In Figure 26, four points of the solution were selected: P_1, P_2, P_3, and P_4. These points represent four different options for the aircraft design. P_1 is the condition where the aircraft has the highest fuel consumption, and it happens when all degrees-of-hybridization are equal to zero ($\psi_{\text{phase}_i} = 0$), i.e., in this case, the configuration represents a turboelectric aircraft. At the other end, P_4 is the condition where the aircraft consumes no fuel, i.e., it implies a full electric configuration; therefore, the aircraft energy is only supplied by batteries, increasing the takeoff weight to the maximum. The points between P_1 and P_4 have different combinations of degrees-of-hybridization and geometry.

Furthermore, the details of the aircraft design optimization for the four points selected are displayed in Tab. 7. The different combinations of the design variables resulted in different weight breakdowns for the aircraft. P_1, for example, requires 73.6 kg of fuel and none battery,

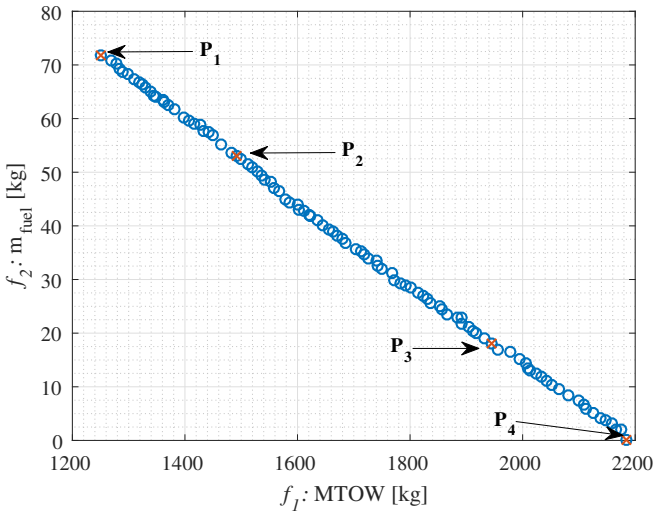

Figure 26 – Pareto-front that represents the solution for the optimization problem.

Table 7 – Results of the optimization.

Parameter	P_1	P_2	P_3	P_4
Airfoil_w	NACA23012	NACA63_1412	NACA63_1412	NACA63_1412
Airfoil_{HT}	AH21	NACA63-012	NACA63-012	NACA63-012
$\mathcal{AR}_w$	15	15	15	15
λ_w	0.40	0.40	0.40	0.40
$\mathcal{AR}_{HT}$	5.6	4.5	4.6	4.2
$c_{root,HT}$	0.57	0.98	0.99	0.79
ψ_{TO}	0.00	0.59	0.84	1.00
ψ_{CL}	0.00	0.21	0.79	1.00
ψ_{CR}	0.00	0.30	0.82	1.00
ψ_{DS}	0.00	0.00	0.35	1.00
ψ_{LT}	0.00	0.60	0.94	1.00
m_{empty} [kg]	711.0	771.6	888.7	949.7
m_{bat} [kg]	0.0	205.0	587.1	777.4
m_{fuel} [kg]	73.6	53.0	18.0	0.0
m_{PT} [kg]	81.8	77.7	66.6	64.5
m_{PL} [kg]	384.0	384.0	384.0	384.0
m_{TO} [kg]	1250.5	1491.3	1944.4	2175.5

since it is turboelectric. But moving forward through the other points, the correlation between fuel and battery mass is not linear, i.e., the amount of batteries increases in a different rate that the fuel amount decreases. This happens because they are directly dependent of the degrees-of-hybridization selected by the algorithm of optimization, along with the respective geometric parameters. The geometry differences, i.e, aspect ratio, wingspan, and tails sizes for the aircraft of points P_1, P_2, P_3, and P_4 are depicted in Fig. 27, and the weight breakdown in Fig. 28.

Since by increasing the amount of batteries there will be a reduction of fuel consumption but a weight increase and the objective-functions were intended to reduce fuel consumption and

(a) Aircraft P_1 - Turboelectric.

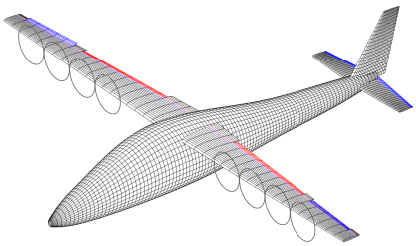

(b) Aircraft P_2 - Hybrid-electric.

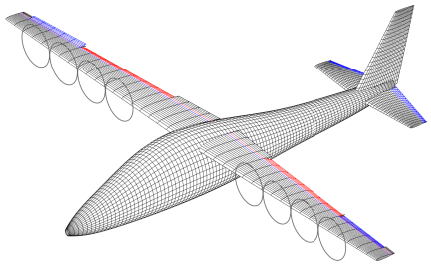

(c) Aircraft P_3 - Hybrid-electric.

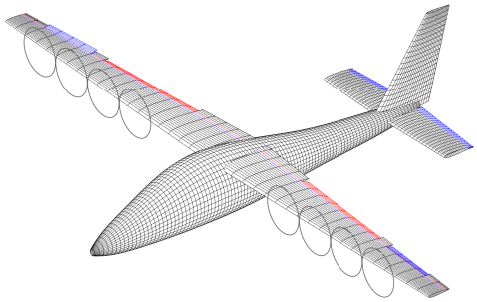

(d) Aircraft P_4 - Full-electric.

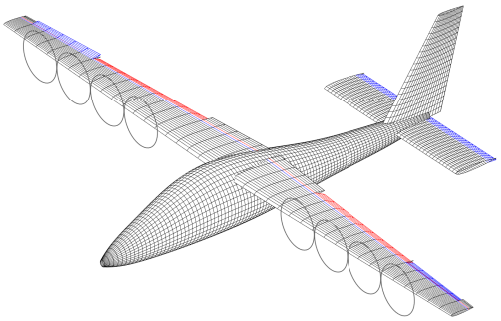

Figure 27 – Illustration of the aircraft obtained from the select points of the Pareto-front.

(a) Aircraft P_1 - Turboelectric.

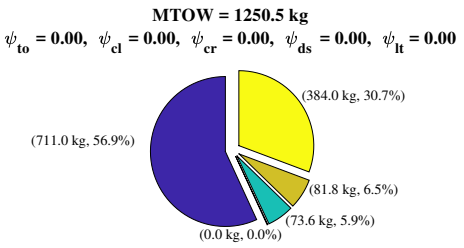

(b) Aircraft P_2 - Hybrid-electric.

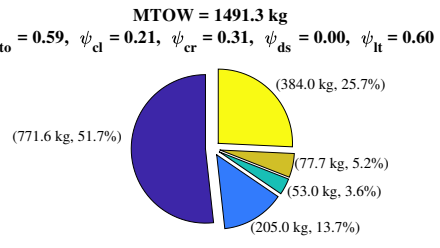

(c) Aircraft P_3 - Hybrid-electric.

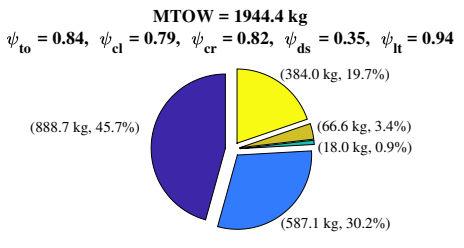

(d) Aircraft P_4 - Full-electric.

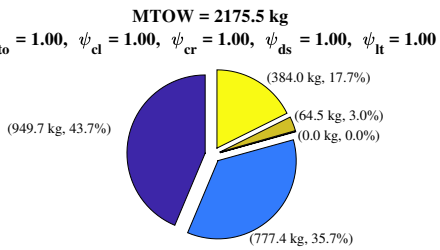

Figure 28 – Weight breakdown of the aircraft obtained from the select points of the Pareto-front.

takeoff weight, the algorithm searched for more efficient aircraft with better aerodynamic behavior in order to reduce the fuel consumption without increase the overall weight. Actually, since the distributed propulsion system brings great improvements in the aero-propulsive interactions and the increase of the lift coefficient by its "Deltas" a higher wing loading was feasible for this design, leading to smaller wing areas for a certain takeoff weight. Moreover, smaller wings result in lighter wings, and, consequently, lighter aircraft weight. Thus, having those aerodynamic improvements, it is much easier to have an aircraft that fulfills the design requirements, but burning less fossil fuel.

Overall, any combination obtained from Fig. 26 results in a different aircraft, with different powertrain, fuel consumption, battery weight, takeoff weight and so on. Therefore, the choice of the point within the Pareto-front depends on what the designer wants to benefit the most.

CHAPTER

6

CONCLUSIONS AND PERSPECTIVES

This work introduces a multi-disciplinary design optimization for conceptual design of general aviation and hybrid-electric aircraft. It was also developed as generic as possible in order to design aircraft to fly short-range missions. The study case presented satisfactory results, mainly in relation to the physical agreement of the models, proving MDO's ability to solve the problem, fulfilling its objective.

The methods presented in each box had been already tested and validated. However, in a multi-disciplinary approach there is the need to ensure that the tools are capable of interact with each other and generate reliable results, so the MDO were validated using the XFLR5 and the OpenVSP that generated very similar aerodynamic and flight mechanics results. Next, a study case was presented for a general aviation aircraft, using geometry and propulsive variables, in order to minimize fuel consumption and the overall weight of the aircraft. The Pareto optimal-front in Fig. 26 comprises aircraft with different propulsive architectures: turboelectric, hybrid-electric, and full-electric. Then, the NSGA II algorithm was able to optimize the aerodynamic characteristics in order to find the best aircraft configuration capable to meet the proposed requirements.

Since the degrees-of-hybridization per flight phase directly affect the final weight break-down of the aircraft, one may realize that full-electric aircraft have their weight considerably increased, mostly because of the high battery demand to accomplish the flight mission. This overweight results in bigger lifting surfaces and, consequently, implies in more structural weight. So, for aircraft with high capacity payload and/or great ranges, such as an intercontinental flight, the amount energy required would be huge, implying in a great increase of weight if batteries were been taking into account. Therefore, the batteries technology needs to be highly improved in the next years in order to enable such approach for this type of design.

For further works, the perspective is to keep increasing the complexity of the MDO by coupling new tools so more innovative designs can be generated. Also, improve the already

existent boxes in order to decreases the elapsed time of every run increase its reliability, which the distributed propulsion analysis is a great example, since there were major simplifications and there is still greater benefits to be explored on this site of research.

BIBLIOGRAPHY

ANDRES, R. J.; GREGG, J. S.; LOSEY, L.; MARLAND, G.; BODEN, T. A. Monthly, global emissions of carbon dioxide from fossil fuel consumption. **Tellus B: Chemical and Physical Meteorology**, Taylor & Francis, v. 63, n. 3, p. 309–327, 2011. Citation on page 25.

CARVALHO, A. R. D. *et al.* Implementação de uma plataforma para análises aerodinâmicas não lineares de aeronaves de geometrias complexas em regime subsônico. Universidade Federal de Uberlândia, 2018. Citations on pages 41, 43, 44, and 48.

CINAR, G.; MAVRIS, D. N.; EMENETH, M.; SCHNEEGANS, A.; FEFERMANN, Y. Development of parametric power generation and distribution subsystem models at the conceptual aircraft design stage. In: **55th AIAA Aerospace Sciences Meeting**. [S.l.: s.n.], 2017. p. 1182. Citation on page 32.

DATTA, S. Efficient genetic algorithm on linear programming problem for fittest chromosomes. **Journal of Global Research in Computer Science**, v. 3, n. 6, p. 1–7, 2012. Citation on page 29.

DEB, K.; AGRAWAL, S.; PRATAP, A.; MEYARIVAN, T. A fast elitist non-dominated sorting genetic algorithm for multi-objective optimization: Nsga-ii. In: SPRINGER. **International conference on parallel problem solving from nature**. [S.l.], 2000. p. 849–858. Citation on page 75.

FELDER, J. L. Nasa electric propulsion system studies. 2015. Citation on page 35.

GERARD, G.; BECKER, H. **Handbook of Structural Stability: Failure of Plates and Composite Elements**. [S.l.]: National Advisory Committee for Aeronautics, 1957. Citation on page 52.

GERSSEN-GONDELACH, S. J.; FAAIJ, A. P. Performance of batteries for electric vehicles on short and longer term. **Journal of power sources**, Elsevier, v. 212, p. 111–129, 2012. Citation on page 33.

GIL A. A.; GUIMARAES, T. A. M. An analytical-based optimization approach to preliminary weight sizing of aircraft wings. Universidade Federal de Minas Gerais, 2006. Citation on page 49.

HESS, J.; SMITH, A. **Calculation of Potential Flow about Arbitrary Bodies," Progress in Aeronautical Sciences, Vol. 8**. [S.l.]: Pergamon Press, Oxford, 1966. Citation on page 44.

KIM, H. D. Distributed propulsion vehicles. 2010. Citations on pages 31 and 36.

KROO, I.; ALTUS, S.; BRAUN, R.; GAGE, P.; SOBIESKI, I. Multidisciplinary optimization methods for aircraft preliminary design. In: **5th symposium on multidisciplinary analysis and optimization**. [S.l.: s.n.], 1994. p. 4325. Citations on pages 25 and 27.

KUHN, H.; SIZMANN, A. **Fundamental prerequisites for electric flying**. [S.l.]: Deutsche Gesellschaft für Luft-und Raumfahrt-Lilienthal-Oberth eV, 2012. Citation on page 31.

MEGSON, T. H. G. **Aircraft structures for engineering students**. [S.l.]: Butterworth-Heinemann, 2016. Citation on page 49.

MIRANDA, E.; ELLIOTT, R. A generalized vortex lattice method for subsonic and supersonic flow applications. **A Generalized Vortex Lattice Method for Subsonic and Supersonic Flow Applications," NASA CR-2865**, 1977. Citation on page 44.

NELSON, R. C. *et al.* **Flight stability and automatic control**. [S.l.]: WCB/McGraw Hill New York, 1998. Citation on page 56.

NICOLAI, L. M.; CARICHNER, G. E. **Fundamentals of aircraft and airship design, volume 1–aircraft design**. [S.l.]: American Institute of Aeronautics and Astronautics, 2010. Citation on page 49.

PRICE, K. V. Differential evolution. In: **Handbook of Optimization**. [S.l.]: Springer, 2013. p. 187–214. Citation on page 30.

RESENDE, G. J. *et al.* A proposal of tail and control surfaces design. Universidade Federal de Uberlândia, 2019. Citations on pages 54 and 58.

RIVELLO, R. M. **Theory and analysis of flight structures**. [S.l.]: McGraw-Hill College, 1969. Citation on page 50.

ROSKAM, J. **Airplane design**. [S.l.]: DARcorporation, 1985. Citations on pages 64 and 68.

SCHILDCROUT, M.; STEIN, M. Critical combinations of shear and direct axial stress for curved rectangular panels. 1949. Citation on page 53.

SILVA, H. L. *et al.* Contributions to conceptual design of electric and hybrid-electric aircraft. Universidade Federal de Uberlândia, 2019. Citations on pages 25, 31, 33, 59, 61, and 63.

SILVA, H. L.; RESENDE, G. J.; NETO, R. M. C.; CARVALHO, A. R. D.; GIL, A. A.; CRUZ, M. A. A.; GUIMARÃES, T. A. M. A multidisciplinary design optimization for conceptual design of general aviation and hybrid-electric aircraft. In: . [S.l.: s.n.], 2019. p. 10. Citations on pages 39, 54, 55, and 59.

SINGH, R.; ISIKVEREN, A.; KAISER, S.; PORNET, C.; VRATNY, P. Pre-design strategies and sizing techniques for dual-energy aircraft. **Aircraft Engineering and Aerospace Technology: An International Journal**, Emerald Group Publishing Limited, 2014. Citation on page 34.

SOBIESZCZANSKI-SOBIESKI, J.; HAFTKA, R. T. Multidisciplinary aerospace design optimization: survey of recent developments. **Structural optimization**, Springer, v. 14, n. 1, p. 1–23, 1997. Citations on pages 25 and 27.

VARGAS, L. A. T. de. Desenvolvimento e implementação de um procedimento numérico para cálculo de conjuntos asa-empenagens de geometria complexa em regime de vôo subsônico, assimétrico e não linear. Universidade Federal de Minas Gerais, 2006. Citation on page 45.

VRIES, R. de; BROWN, M. T.; VOS, R. A preliminary sizing method for hybrid-electric aircraft including aero-propulsive interaction effects. In: **2018 Aviation Technology, Integration, and Operations Conference**. [S.l.: s.n.], 2018. p. 4228. Citation on page 38.

ZAMBONI, J.; VOS, R.; EMENETH, M.; SCHNEEGANS, A. A method for the conceptual design of hybrid electric aircraft. In: **AIAA Scitech 2019 Forum**. [S.l.: s.n.], 2019. p. 1587. Citation on page 33.